Cancer & Metabolism

RESEARCH Open Access

Immunogenic shift of arginine metabolism triggers systemic metabolic and immunological reprogramming to suppress HER2 + breast cancer

Vandana Sharma[1,2], Veani Fernando[1,3], Xunzhen Zheng[1], Eun-Seok Choi[4], Osama Sweef[4], Venetia Thomas[4], Justin Szpendyk[4] and Saori Furuta[1,4*]

Abstract

Background Arginine metabolism in tumors is often shunted into the pathway producing pro-tumor and immune suppressive polyamines (PAs), while downmodulating the alternative nitric oxide (NO) synthesis pathway. Aiming to correct arginine metabolism in tumors, arginine deprivation therapy and inhibitors of PA synthesis have been developed. Despite some therapeutic advantages, these approaches have often yielded severe side effects, making it necessary to explore an alternative strategy. We previously reported that supplementing sepiapterin (SEP), the endogenous precursor of tetrahydrobiopterin (BH_4, the essential NO synthase cofactor), could correct arginine metabolism in tumor cells and tumor-associated macrophages (TAMs) and induce their metabolic and phenotypic reprogramming. We saw that oral SEP treatment effectively suppressed the growth of HER2-positive mammary tumors in animals. SEP also has no reported dose-dependent toxicity in clinical trials for metabolic disorders. In the present study, we tested our hypothesis that a long-term administration of SEP to individuals susceptible to HER2-positive mammary tumor would protect them against tumor occurrence.

Methods We administered SEP, in comparison to control DMSO, to MMTV-neu mice susceptible to HER2-positive mammary tumors for 8 months starting at their pre-pubertal stage. We monitored tumor onsets to determine the rate of tumor-free survival. After 8 months of treatment, we grouped animals into DMSO treatment with or without tumors and SEP treatment with or without tumors. We analyzed blood metabolites, PBMC, and bone marrow of DMSO vs. SEP treated animals.

Results We found that a long-term use of SEP in animals susceptible to HER2-positive mammary tumors effectively suppressed tumor occurrence. These SEP-treated animals had undergone reprogramming of the systemic metabolism and immunity, elevating total T cell counts in the circulation and bone marrow. Given that bone marrow-resident T cells are mostly memory T cells, it is plausible that chronic SEP treatment promoted memory T cell formation, leading to a potent tumor prevention.

Conclusions These findings suggest the possible roles of the SEP/BH_4/NO axis in promoting memory T cell formation and its potential therapeutic utility for preventing HER2-positive breast cancer.

Keywords Breast cancer, Arginine, Metabolism, HER2, Cancer prevention, Nitric oxide, Polyamines, T cells

*Correspondence:
Saori Furuta
sxf494@case.edu
Full list of author information is available at the end of the article

Introduction

Arginine is a semi-essential amino acid mainly obtained from outside sources [1] and is mostly metabolized into two opposing pathways: nitric oxide (NO) vs. polyamine (PA) syntheses [2–5]. In tumors, arginine tends to be converted to PAs, small polycationic metabolites essential for cell growth and immune suppression [6, 7]. High levels of PAs help establish the "cold" tumor microenvironment (TME). For example, PAs inhibit formation of cytotoxic (CD8+) memory T cells, compromising immunological responses [7]. In addition, tumor-associated macrophages (TAMs), primarily polarized to the immune suppressive M2-type, preferentially produce PAs from arginine, further elevating PA levels in TME [8–10]. Such predominance of PA synthesis in tumors is primarily mediated by suppression of the alternative NO synthesis pathway. This is largely due to reduced availability of tetrahydrobiopterin (BH_4), the essential NO synthase (NOS) cofactor which is often targeted for oxidative inactivation [11]. We also showed that pharmacological inhibition of NO in normal mammary glands of wild-type mice induced the formation of precancerous lesions that highly expressed HER2, indicating a potential pathogenic relevance of NO inhibition to HER2+breast cancer [12]. Consistently, by using cell lines of the MCF10A human breast cancer progression series, we showed that cancer progression was closely linked to declines of basal NO and BH_4 production, along with increases of HER2 and cell proliferation markers [12].

Aiming to correct arginine metabolism in cancer, different strategies have been explored in clinical trials, including arginine deprivation therapy and PA synthesis inhibition [6, 13, 14]. Despite some therapeutic benefits, these methods have yielded serious adverse side effects limiting their usages [15, 16]. Thus, there is a critical need to develop a less toxic strategy to normalize arginine metabolism in cancer patients. We have been testing the effect of sepiapterin (SEP), the endogenous BH_4 precursor, on modulating arginine metabolism in breast tumors and tumor-susceptible individuals and determining its therapeutic efficacy. SEP has been extensively utilized for treating metabolic syndrome, such as phenylketonuria, and exhibited no dose-limiting toxicity during the Phase I trial [17] unlike other modulators of arginine metabolism [15, 16]. We previously showed that supplementing SEP to breast cancer cells effectively suppressed PA production, while elevating NO synthesis and also downmodulating HER2 and cell proliferation to the levels similar to normal cells [12, 18]. We also showed that SEP treatment of the immuno-suppressive M2-type TAMs lowered PA production, while elevating NO production, leading to their functional conversion to the pro-immunogenic M1-type TAMs [18, 19]. These reprogrammed TAMs, in turn, activated anti-tumor activity of cytotoxic T cells, leading to significant suppression of HER2+mammary tumor growth [19].

In the present study, we explored our hypothesis that chronic oral SEP treatment of animals susceptible to HER2+breast tumors might prevent or prolong the tumor occurrence. We found that a long-term oral administration of SEP to a mouse model of HER2-positive mammary tumors strongly prevented tumor formation. As the mechanistic basis of this phenomenon, we observed that SEP induced reprogramming of the systemic metabolism and immunity, elevating total T cell populations in the circulation and bone marrow. Specifically, bone marrow-resident T cells are known to largely consist of memory T cells [20–22], indicating the ability of SEP to promote memory T cell formation as part of its tumor preventative capabilities. These findings suggest the therapeutic efficacy of a long-term use of SEP in promoting anti-tumor metabolism and immunity for protection of individuals susceptible to HER2-positive mammary tumors.

Materials & methods

Cell lines

Human monocytic THP–1 cells (Cat. No. TIB-202™) were purchased from American Type Culture Collection (ATCC). MCF10A human breast epithelial cells and CA1d human breast cancer cells were obtained from Karmanos Cancer Institute (Detroit, MI) under Material Transfer Agreement (MTA). Peripheral blood mononuclear cells (PBMCs) were obtained from Stemcell Technologies (Vancouver, BC, Canada) and AllCells LLC (Alameda, CA).

Cell culture & reagents

THP–1 cells were maintained at a density of 1×10^6 cells/ml in RPMI 1640 Medium (Thermo Fisher, Waltham, MA, Cat. No. 11835055) supplemented with 10% fetal bovine serum (FBS), 1% Penicillin/Streptomycin, 2 mM GlutaMAX™, 10 mM HEPES buffer, 45 g/L Glucose and 1 mM Sodium Pyruvate (Thermo Fisher, Cat. No. 15140122, Cat. No. 35050061, Cat. No. SH3023701, Cat. No. A2494001 & Cat. No. 11–360-070). PBMCs were plated at a density of 1.5×10^6 cells/ml in RPMI serum-free medium and incubated for 3 h. Monocytes were then isolated based on their adhesion to plastic. Serum-free medium was aspirated to remove non–adherent cells. Subsequently, the adherent monocytic cells were replenished with RPMI medium containing 20% FBS and maintained for 24 h before use. MCF10A and CA1d cells were cultured in DMEM/F12 medium with 5% Horse serum, 1% Penicillin/Streptomycin, 20 ng/ml Epidermal Growth Factor (EGF, Thermo Fisher/Gibco/Peprotech, Cat. No.

GMP100-15-100UG), 0.5 µg/ml Hydrocortisone, 100 ng/ml Cholera Toxin, and 10 µg/ml Insulin (Sigma-Aldrich, Inc, St. Louis, MO, Cat. No. H-0888, Cat. No. C8052-2MG & Cat. No. I1882) [23]. All the cells were maintained in a 37 °C humidified incubator with 5% CO_2.

Antibodies

Here are the antibodies used: Primary antibodies for western blot, anti-human CD163 (Abcam, Cat. No. ab182422), anti-human TNFα (Thermo Fisher, Cat. No. MA523720), and anti-human β–Actin (Sigma-Aldrich, Cat. No. A1978); secondary antibodies for western blot, horseradish peroxidase (HRP) conjugated Sheep anti-Mouse IgG (GE Healthcare Life Sciences, Pittsburgh, PA, Cat. No. NA931-1ML), Donkey anti-Rabbit IgG (GE Healthcare Life Sciences, Cat. No. NA934-1ML), and Donkey anti-Goat IgG (Thermo Fisher, Cat. No. A16005); primary antibodies for FACS, anti-human Ki67 (BioLegend, Cat. No. 350504), anti-human CD68 (BioLegend, Cat. No. 333821), anti-human CD40 (BioLegend, Cat. No. 334305), anti-human CD80 (BioLegend, Cat. No. 305205), anti-human CD163 (BioLegend, Cat. No. 333609), anti-human CD206 (BioLegend, Cat. No. 321109), anti-human TNFα (BioLegend, Cat. No. 502943), anti-mouse F4/80 (BioLegend, Cat. No. 123118), anti-mouse CD80 (BioLegend, Cat. No. 104706), and anti-mouse CD163 (BioLegend, Cat. No. 155320); and for CUT&Tag analysis, anti-H3K27me3 and anti-H3K27Ac antibody (Active Motif 39,156, 23,254,116–11; Active Motif 39,135, 23,061,102–11).

Modulation of arginine metabolism

For the induction of NO production, we used SEP, a precursor of NOS cofactor tetrahydrobiopterin (BH_4) (20 or 100 µM, Career Henan Chemical Co). For NO inhibition, we used the NOS2 inhibitor: 1400W hydrochloride (100 µM, Cayman Chemical, Ann Arbor, MI, Cat. No. 81520). For inhibition of PAs, we used an inhibitor of Arginase I, N-hydroxy-nor-L-arginine (nor-NOHA, 50 µM, Cayman Chemical, Ann Arbor, MI, Cat. No. 10006861).

In vitro model of TAMs

Human monocytic THP–1 cells were seeded at a density of 3×10^5 cells/ml and treated with 100 ng/ml phorbol myristate acetate (PMA, InvivoGen, San Diego, CA, Cat. No. tlrl-pma) for 24 h for their differentiation to nascent (M0) macrophages. M0 cells were then serum-starved for 2 h in X-VIVO™ hematopoietic cell medium (Lonza, Basel, Switzerland, Cat. No. BEBP04-744Q). For M1 polarization (M1-TAMs), M0 cells were treated with PMA (100 ng/ml), 5 ng/ml lipopolysaccharide (LPS, Sigma-Aldrich, Cat. No. L4391-1MG), and 20 ng/ml interferon γ (IFNγ, PeproTech, Cranbury, NJ, Cat. No. 300–02) for 66 h. For M2 polarization (M2-TAMs), M0 cells were treated with PMA (100 ng/ml), 20 ng/ml interleukin 4 (IL4, PeproTech, Cat. No. 200–04), and 20 ng/ml interleukin 13 (IL13, PeproTech, Cat. No. 200–13) for 66 h [19].

PBMCs were plated at a density of 1.5×10^6 cells/ml in RPMI serum-free medium and incubated for 3 h. Monocytes were isolated based on their adhesion to plastic. Serum-free medium was aspirated to remove non–adherent cells. The adherent cells were replenished with RPMI medium containing 20% FBS and incubated for 24 h. Non–adherent cells were further removed by washing with pre–warmed RPMI medium. To induce M0 macrophage differentiation, the remaining adherent cells were treated with 10 ng/mL recombinant Skp/Cullin/F-box (SCF) protein (Stem Cell Factor, Peprotech, Cat. No. 300–07-10UG) and 50 ng/mL granulocyte macrophage colony stimulating factor (GM–CSF, for M1 polarization) or 50 ng/mL macrophage colony-stimulating factor (M–CSF, for M2 polarization) (BioLegend, San Diego, CA, Cat. No. 573904, Cat. No. 572903 and Cat. No. 574804) for 7 days with 50% medium replenishment every 3 days. Upon differentiation, M0 cells were starved for 2 h as described above and given M1 or M2 polarization treatment as described above for 3 days [19].

Reprogramming of M2–macrophages to M1-macrophages

THP–1 or PBMC-derived M2–macrophages were treated with 100 µM SEP (Career Henan Chemical Co., Zhengzhou City, China, CAS No. 17094–01–8) with daily medium change for 3 days for reprogramming to M1 macrophages. M2–macrophages were also treated with DMSO (Vehicle) and 5 ng/ml LPS and 20 ng/ml IFNγ as negative and positive controls, respectively.

Immunoblotting

Cell lysates were prepared using the following lysis buffer: 25 mM Tris–HCl (pH 8), 150 mM NaCl, 1 mM EDTA (pH 8), 1% NP–40, 5% Glycerol, 1X PhosSTOP (Sigma-Aldrich, Cat. No. 4906837001) and 1X Protease Inhibitor Cocktail (Thermo Fisher, Cat. No. 78425). Total protein concentration of the cell lysates was quantified using the Pierce BCA Protein Assay Kit (Thermo Fisher, Cat. No. 23227). Cell lysates were mixed with the sample buffer (with beta-mercaptoethanol) boiled at 100 °C for 10 min. Proteins were separated by sodium dodecyl-sulfate polyacrylamide gel electrophoresis (SDS-PAGE). The separated proteins were then electroblotted to methanol–activated polyvinylidene fluoride (PVDF) membranes (Sigma-Aldrich, Cat. No. IPVH00010). Upon transfer, membranes were blocked with 5% non-fat milk in Tris-buffered saline containing 0.1% Tween® 20 (TBST) and incubated overnight with the following

primary antibodies: anti-human CD163 (Abcam, Cat. No. ab182422), anti-human TNFα (Thermo Fisher, Cat. No. MA523720), and anti-human β–Actin (Sigma-Aldrich, Cat. No. A1978). Then they were incubated with horseradish peroxidase (HRP) conjugated Sheep anti-Mouse IgG (GE Healthcare Life Sciences, Pittsburgh, PA, Cat. No. NA931-1ML), Donkey anti-Rabbit IgG (GE Healthcare Life Sciences, Cat. No. NA934-1ML) or Donkey anti-Goat IgG (Thermo Fisher, Cat. No. A16005) secondary antibodies (1:5000 dilution). Next, the blots were developed with SuperSignal™ West Dura Extended Duration Substrate (Thermo Fisher, Cat. No. 34076) and imaged using Syngene G:BOX F3 gel doc system.

Flow cytometry (FACS) analysis of cell surface markers

Cells were dissociated from culture plates through incubation with PBS containing 5 mM EDTA for 15 min at 37 °C, followed by gentle scraping. Cells were collected into 96 well V bottom plates (USA Scientific, Ocala, FL, Cat. No. 5665–1101) and centrifuged at 1000 rpm for 5 min. Cell pellets were washed with Fluorescence-activated cell sorting (FACS) buffer (PBS, 2% FBS) and blocked for 30 min on ice in the blocking buffer: 2% FBS, 2% goat serum, 2% rabbit serum, and 10 μg/mL human Immunoglobulin G (IgG). Cells were then incubated with fluorochrome-labeled antibodies prepared in FACS buffer for 1 h on ice. The antibodies used are as follows: anti-human CD68 (BioLegend, Cat. No. 333821), anti-human CD40 (BioLegend, Cat. No. 334305), anti-human CD80 (BioLegend, Cat. No. 305205), anti-human CD163 (BioLegend, Cat. No. 333609), anti-human CD206 (BioLegend, Cat. No. 321109), anti-mouse F4/80 (BioLegend, Cat. No. 123118), anti-mouse CD80 (BioLegend, Cat. No. 104706), and anti-mouse CD163 (BioLegend, Cat. No. 155306). Cells were washed twice with FACS buffer and resuspended in Dulbecco's phosphate-buffered saline (DPBS) containing 2% formaldehyde. Samples were assayed on the BD FACSCanto™ II system, followed by analyses with FlowJo software.

FACS analysis of intracellular markers

Cultured cells were treated with 1 μg/ml Brefeldin A (Fisher Scientific, Cat. No. B7450) for 5 h at 37 °C. Cells were collected into 96 well V bottom plates and centrifuged as described above. The samples were then incubated with 1X Fixation/Permeabilization Buffer (R&D systems, Cat. No. FC007) for 12 min at 4 °C. Following fixation, samples were centrifuged at 1600 rpm for 5 min and washed with the Permeabilization/Washing buffer: PBS, 2% FBS and 0.1% Triton X-100. Samples were then blocked with blocking buffer containing 0.1% Triton X-100 for 10 min. After blocking, samples were incubated with fluorochrome-labeled antibodies prepared in permeabilization/washing buffer for 45 min at 4 °C. The following antibodies were used: Anti-human Ki67 (BioLegend, Cat. No. 350504) and anti-human TNFα (BioLegend, Cat. No. 502943) for cultured human cells; anti-mouse IL12 (BioLegend, Cat. No. 505206), anti-mouse IL10 (BioLegend, Cat. No. 505006) for mouse tumors. Following antibody incubation, samples were washed with permeabilization/washing buffer, resuspended in DPBS containing 2% formaldehyde and assayed on the BD FACSCanto™ II system, followed by analyses with FlowJo software.

Measurement of BH_4 production

Cells were washed with ice-cold PBS to remove the remaining medium. Upon washing, cells were scraped gently, and the cell pellets were collected to Eppendorf™ tubes. The cell pellets were vortexed for 10 s and flash frozen in liquid nitrogen (N_2). Then the pellets were thawed at RT. The process was repeated 5 times. Then the pellets were centrifuged at 1000 rpm for 5 min, and the supernatants were collected into fresh tubes. The BH_4 level in cell lysate was measured using an enzyme–linked immunosorbent assay (ELISA) Kit (Abbexa, Sugar Land, TX, Cat. No. abx354211) following manufacturer's protocol. Cellular BH_4 levels were normalized using the total protein concentration in cell lysates.

Measurement of cytokine secretion

Cells were cultured in RPMI serum-free medium for 2 days following treatment and the conditioned meda (CM) were collected. Secreted cytokines in the CM were quantified using ELISA kits according to manufacturers' protocol. The ELISA kits used were as follows: human IL12 (R&D systems, Cat. No. D1200) and human IL10 (R&D systems, Cat. No. D1000B).

Animal study

All in vivo experiments were performed in compliance to The Guide for the Care and Use of Laboratory Animals (National Research Council, National Academy Press, Washington, D.C., 2010) and with the approval of the Institutional Animal Care and Use Committee of the University of Toledo, Toledo, OH (Protocol No: 108658) and Case Western Reserve University, Cleveland, OH (Protocol No. 2022–0080). We only used female mice as animal models of breast cancer which predominantly affects females. (Besides, spontaneous mammary tumor growth in the animal model we used, MMTV-neu/FVB, is only seen for females.)

For tumor treatment study, two months old female MMTV-neu/FVB (unactivated) ($n=14$) mice were obtained from the Jackson Laboratory (ID. IMSR_JAX:002376,

Bar Harhor, MN, USA), housed under regular conditions and given ad libitum access to acidified water and regular chow. Mice were maintained until spontaneous mammary tumors became palpable (~5 mm long, 6–14 months). Upon tumor onset, mice were divided into vehicle (DMSO) vs. SEP (10 mg/kg) treatment groups (n=7/treatment) [24, 25]. The drugs were dissolved in acidified drinking water and administered to mice ad libitum for 6 weeks [26]. Tumor growth, body weight and morbidity of the animals were monitored twice a week. Tumor volume was calculated by the modified ellipsoidal formula: Volume = (Length x Width x Width) x ½. At the end of treatment, mice were euthanized, and mammary tumors were processed for further analyses described below.

For tumor prevention study, four weeks old female MMTV-neu/FVB (unactivated) (n=40) mice were obtained from the Jackson Laboratory (ID. IMSR_JAX:002376, Bar Harhor, MN, USA), housed under regular conditions and given ad libitum access to acidified water and regular chow. For drug treatment, animals were assigned to experimental groups using simple randomization. They were divided into vehicle (DMSO) vs. SEP (1 mg/kg) treatment group (n=20/treatment). The drugs were dissolved in acidified drinking water and administered to mice ad libitum starting at 5 weeks of age for 8 months. Tumor occurrence was monitored, and the percentage of tumor-free mice was quantified. The body weight, tumor incident, latency and size were monitored twice a week, and urine and fecal samples were collected once every three weeks. All measurements were performed blinded, and data analyzers were unaware of the nature of treatments. If animals met early termination criteria (e.g., morbidity and tumor size > 1500 mm^3), they were euthanized. However, for construction of tumor-free survival curves, the data of all animals (total of 40) were included, and there was no attrition for treatments. At the end of treatment, mammary tumors, spleens, livers, bone marrows, and blood were harvested and processed for further analyses.

Profiling of macrophages in tumors

Freshly harvested tumors were processed for the profiling of resident macrophages. Tumors were weighed to obtain 1.5 ~ 2 g fragments/sample and reacted in the digestion mixture [10 ml/g of tissue, 3 mg/ml Collagenase A (Sigma, Cat. No. 10103578001) and 25 µg/ml DNase I (Sigma, Cat. No. 10104159001)] in Hanks' Balanced Salt Solution (HBSS, Thermo Fisher, Cat. No. 14025092) with gentle motions on a platform shaker for 45 min at 37 °C [27]. To stop the enzymatic digestion, the samples were treated with 10 ml of staining buffer (1% (w/v) BSA in PBS). Cell suspension was then filtered through a 100 µm-cell strainer, and the volume was adjusted to 20 ml with staining buffer. Then, cells were pelleted by centrifugation at 500 × g for 7 min at 4 °C. To remove red blood cells, the pelleted cells were suspended in 3 ml of 1X Red Blood Cell (RBC) lysis buffer (Thermo Fisher, Cat. No. 00–4300-54) and incubated on ice for 10 min. A volume of 30 ml of staining buffer was added; cells were centrifuged and resuspended in 1 ml of staining buffer. To block Fc receptors (to avoid unwanted antibody binding), cells were treated with 2 µl of anti-mouse CD16 (FcγII)/CD32 (FcγIII) Antibody (Thermo Fisher, Cat. No. 14–0161-82) and incubated on ice for 30 min with mixing at 10 min intervals. A volume of 4 ml of staining buffer was added, and samples were centrifuged at 500 × g for 5 min at 4 °C. Then, cell pellets were resuspended in 1 ml of staining buffer [28]. Cells were then stained with relevant fluorochrome labeled antibodies and analyzed by FACS analysis (see above).

PBMC isolation from mouse blood

At the end of tumor prevention experiment, MMTV-neu/FVB mice were grouped into four groups (DMSO with tumors, DMSO without tumors, SEP with tumors, and SEP without tumors). Whole blood was collected by cardiac puncture into EDTA-coated collection tubes, pooled by group, and mixed with the equal volume of PBS-EDTA solution (Thermo Fisher, Cat. No. J60893.K3). To isolate mononuclear cells, the diluted blood was added on top of Lymphoprep medium (STEMCELL technologies, Cat. No. 07851) within a SepMate-15 centrifuge tube (STEMCELL technologies, Cat. No. 85415) and spun at 1200 × g for 10 min at room temperature for density gradient centrifugation. Mononuclear cells accumulated at the interface between the top serum and bottom Lymphoprep layers were carefully collected and transferred into a separate centrifuge tube. Cells were washed in PBS plus 2% FBS twice, resuspended in RPMI-1640 medium, and cryopreserved until single cell sequencing.

Single cell sequencing

Single cell sequencing was performed with GEM-X Chromium Single Cell Gene Expression (3′ GEX V3.1) chips on 10X genomics Chromium X Processor at the Discovery Lab in the Global Center for Immunotherapy and Precision Immuno-Oncology at Lerner Research Institute, Cleveland Clinic. Fastq files were mapped to the GRCh38 reference human genome using Cell ranger (v5.0.0) [29]. Cells containing less than 600 genes and/or more than 30% mitochondrial and ribosomal genes were removed. Sample-specific Seurat objects were created using Seurat (v4.3.0) [30], then normalized using Seurat's SCTransform method. Samples were integrated based on variable features using Seurat's IntegrateData function. To help predict cell types, Seurat object was uploaded

to BioTuring BbrowserX [31], and cells were annotated using their deep learning-based mouse cell type prediction model (Sub-cell type (Version 2) model). BBrowserX was also used to create UMAPs, differentially expressed gene sets, and Chord diagrams.

Metabolite sample preparation for metabolomic analysis

For the metabolomic analysis of cells, $1–2 \times 10^6$ cells each were frozen in freezing solution (90% FBS + 10% DMSO) and stored at − 80 °C. For the metabolomic analysis of plasma, the whole blood was collected from mice into EDTA-treated tubes. Blood was centrifugated at 2000 g for 20 min at 4 °C and then plasma was recovered as the supernatant and stored at − 80 °C. Cell and plasma samples were subjected to untargeted metabolomics analysis at Metabolon, Inc. (Durham, NC, USA).

Analytes were prepared using the automated MicroLab STAR® system (Hamilton Company, Reno, NV, USA). Briefly, samples were thawed and deproteinized by the addition of fourfold volume of precooled (dry ice) 80% (v/v) methanol extraction solvent containing recovery standard compounds [32]. To remove protein, the mixtures were vortexed, incubated with vigorous shaking for 2 min on Glen Mills GenoGrinder 2000 and centrifuged at 15,000 g at for 30 min 4 °C, and the supernatants were collected. The resulting extract was divided into five fractions: two for analysis by two separate reverse phase (RP)/UPLC-MS/MS methods with positive ion mode electrospray ionization (ESI), one for analysis by RP/UPLC-MS/MS with negative ion mode ESI, one for analysis by HILIC/UPLC-MS/MS with negative ion mode ESI, and one sample was reserved for backup. Samples were placed briefly on a TurboVap® (Zymark) to evaporate the organic solvent. The sample extracts were stored overnight under nitrogen before preparation for analysis.

Metabolomic analysis

Metabolomic analysis was performed on Ultrahigh Performance Liquid Chromatography-Tandem Mass Spectroscopy (UPLC-MS/MS). All methods utilized a Waters ACQUITY ultra-performance liquid chromatography (UPLC) and a Thermo Scientific Q-Exactive high resolution/accurate mass spectrometer interfaced with a heated electrospray ionization (HESI-II) source and Orbitrap mass analyzer operated at 35,000 mass resolution.

The sample extract was dried and then reconstituted in solvents compatible with each of the following four methods. Each reconstitution solvent contained a series of standards at fixed concentrations to ensure injection and chromatographic consistency. The first aliquot was analyzed using acidic positive ion conditions, chromatographically optimized for more hydrophilic compounds. In this method, the extract was gradient eluted from a C18 column (Waters UPLC BEH C18-2.1 × 100 mm, 1.7 µm) using water and methanol, containing 0.05% perfluoropentanoic acid (PFPA) and 0.1% formic acid (FA). The second aliquot was also analyzed using acidic positive ion conditions; however, it was chromatographically optimized for more hydrophobic compounds. In this method, the extract was gradient eluted from the same aforementioned C18 column using methanol, acetonitrile, water, 0.05% PFPA and 0.01% FA and was operated at an overall higher organic content. The third aliquot was analyzed using basic negative ion optimized conditions using a separate dedicated C18 column. The basic extracts were gradient eluted from the column using methanol and water, however with 6.5 mM Ammonium Bicarbonate at pH 8. The fourth aliquot was analyzed via negative ionization following elution from a HILIC column (Waters UPLC BEH Amide 2.1 × 150 mm, 1.7 µm) using a gradient consisting of water and acetonitrile with 10 mM Ammonium Formate, pH 10.8. The MS analysis alternated between MS and data-dependent MSn scans using dynamic exclusion. The scan range varied slightly between methods but covered 70–1000 m/z. Raw data files are archived and extracted as described below.

Metabolomic data analysis

The bioinformatics system consisted of four major components: the Laboratory Information Management System (LIMS), the data extraction and peak-identification software, data processing tools for quality control (QC) and compound identification, and a collection of information interpretation and visualization tools for use by data analysts. Metabolon LIMS system enables fully auditable laboratory automation that encompasses sample accessioning, sample preparation and instrumental analysis and reporting and advanced data analysis. All of the subsequent software systems are grounded in the LIMS data structures. The hardware and software foundations for these informatics components were the LAN backbone, and a database server running Oracle 10.2.0.1 Enterprise Edition.

Raw data was extracted, peak-identified and QC processed using Metabolon's hardware and software built on a web-service platform utilizing Microsoft's.NET technologies. Compounds were identified by comparison to library entries of purified standards or recurrent unknown entities. Metabolon maintains a library based on authenticated standards that contains the retention time/index (RI), mass-to-charge ratio (m/z), and chromatographic data (including MS/MS spectral data) on all molecules present in the library. Biochemical identifications are based on retention index within a narrow RI window of the proposed identification, accurate mass match to the library ± 10 ppm, and the MS/MS forward

and reverse scores between the experimental data and authentic standards. The MS/MS scores are based on a comparison of the ions present in the experimental spectrum to the ions present in the library spectrum. The use of all three data points can be utilized to distinguish and differentiate biochemicals. More than 3300 commercially available purified standard compounds have been registered into LIMS for analysis on all platforms. Additional mass spectral entries have been created for structurally unnamed biochemicals which have the potential to be identified by future acquisitions.

A variety of curation procedures were carried out to ensure that a high-quality data set was made available for statistical analysis and data interpretation. The QC and curation processes were designed to ensure accurate and consistent identification of true chemical entities, and to remove those representing system artifacts, mis-assignments, and background noise.

Peaks were quantified using area-under-the-curve. For studies spanning multiple days, a data normalization step was performed to correct variation resulting from instrument inter-day tuning differences. Essentially, each compound was corrected in run-day blocks by registering the medians to equal one (1.00) and normalizing each data point proportionately (termed the "block correction"). For studies that did not require more than one day of analysis, no normalization is necessary, other than for purposes of data visualization. In certain instances, biochemical data may have been normalized to an additional factor (e.g., cell counts, total protein as determined by Bradford assay, osmolality, etc.) to account for differences in metabolite levels due to differences in the amount of material present in each sample.

Further bioinformatics analyses on curated data, including pathway analyses and ROC curve analyses were performed using the Metaboanalyst 6.0 package (McGill University, Montreal, Quebec, Canada) [33]. Heatmaps were created using the SRPLOT software, while volcano plots were created using Graphpad Prizm Version 10.5.

Cut & Tag analysis of bone marrow cells

Bone marrows of drug treated animals were subjected to CUT & Tag analysis by Active Motif (Carlsbad, CA, USA). Analytes were prepared as previously described with modifications [34]. Briefly, frozen cell pellets were thawed, and nuclei were isolated and incubated overnight with Concanavalin A beads and 1.3 µl of the primary anti-H3K27me3 or anti-H3K27Ac antibody (Active Motif 39156, 23254116–11; Active Motif 39135, 23061102–11) per reaction. After incubation with the secondary anti-rabbit antibody (1:100), beads were washed, and tagmentation was performed at 37℃ using protein-A-Tn5. Tagmentation was halted by the addition of EDTA, SDS and proteinase K after which DNA extraction, and ethanol purification was performed, followed by PCR amplification and barcoding (see Active Motif CUT&Tag kit, Cat. No. 53160 for recommended conditions and indexes). Following SPRI bead cleanup (Beckman Coulter), the resulting DNA libraries were quantified and sequenced on Illumina's NextSeq 550 (8 million reads, 38 paired end). Reads were aligned using the BWA algorithm (mem mode; default settings) to the mouse genome (mm10) [35]. Duplicate reads were removed, and only reads that mapped uniquely (mapping quality $>=1$) and as matched pairs were used for further analysis. Alignments were extended in silico at their 3'-ends to a length of 200 bp and assigned to 32-nt bins along the genome. The resulting histograms (genomic "signal maps") were stored in bigWig files. Peaks were identified using the MACS 3.0.0 algorithm in bedpe mode at a cutoff of q-value 0.05, without control file, and with the –no lambda option. Peaks that were on the ENCODE blacklist of known false ChIPSeq peaks were removed. Signal maps and peak locations were used as input data to Active Motifs proprietary analysis program, which creates Excel tables containing detailed information on sample comparison, peak metrics, peak locations and gene annotations. For differential analysis, reads were counted in all merged peak regions (using Subread), and the replicates for each condition were compared using DESeq2 [36]. Other key software used were as follows: bcl2fastq2 (v2.20) (processing of Illumina base-call data and demultiplexing); Samtools (v0.1.19) (processing of BAM files); BEDtools (v2.25.0) (processing of BED files); wigToBigWig (v4) (generation of bigWIG files); and Subread (v1.5.2) (counting of reads in BAM files for DESeq2).

The data (BED files) were visualized by using the custom-track function of UCSC Genome Browser and specifying specific genomic regions of interest. The pathway analyses of differentially expressed gene sets were performed using the Metascape software. Cell analyses based on epigenomic profiles were performed using the Cellkb software (Combinatics, Ltd.).

Statistical data analysis

All the experiments were performed in replicates ($n \geq 3$ for in vitro analyses, $n=20$ for treatment study in animals, and $n=7$ for animal tissue analyses) ensuring the adequate statistical power (power ≥ 0.8; error ≤ 0.05; and effect size ≥ 0.8, calculated with G*Power) based on our previous studies [37, 38]. Statistical analyses were performed using Graphpad Prism 10.5, and unless otherwise indicated, two-tailed t-tests, Mann–Whitney U test (non-parametric), or two-way ANOVA test with Bonferroni post hoc test (multi-comparisons) [39] were performed to obtain the statistical significance of the

mean difference. *P* values ≤ 0.05 were considered statistically significant. Flow cytometry data analyses were performed using FlowJo Version 10.5.

Results

Reprogramming arginine metabolism inhibits HER2 + breast cancer cell growth

Arginine is a semi-essential amino acid mainly obtained from outside sources [1] and is mostly metabolized into two opposing pathways: NO vs. PA syntheses (Fig. 1A) [2–5]. In cancer, arginine tends to be converted to PAs, promoting cancer cell growth and immune suppression [6, 7]. Elevated PA synthesis is largely due to reduced NO synthesis owing to the lower availability of tetrahydrobiopterin (BH_4), the essential NO synthase cofactor (Fig. 1A) [12, 18]. We previously showed that pharmacological inhibition of NO, which would direct arginine metabolism towards PA synthesis, in normal mammary glands of mice induced the formation of precancerous lesions that highly expressed HER2, indicating a pathogenic relevance of NO inhibition to HER2 + breast cancer [12]. By using MCF10A human breast cancer progression series (normal MCF10A > > cancerous CA1d), we found that cancer progression of this series was also linked to declines of basal BH_4 and NO production (Fig. 1B) as well as the increases in the levels of HER2 and a proliferation marker Ki67 [12]. Conversely, when CA1d cancer cells were treated with SEP (the endogenous BH_4 precursor) (Fig. 1C), BH_4 and Ki67 levels were normalized to the levels of normal MCF10A cells (Fig. 1D, E) [12]. SEP treatment of the cancer progression series lowered PA levels, while elevating NO levels, inducing the shift of arginine metabolism from PA to NO syntheses [18]. In addition to arginine metabolism, SEP treatment of CA1d cells normalized the levels of a group of other metabolites to the levels of MCF10A cells, greatly differentiating their levels

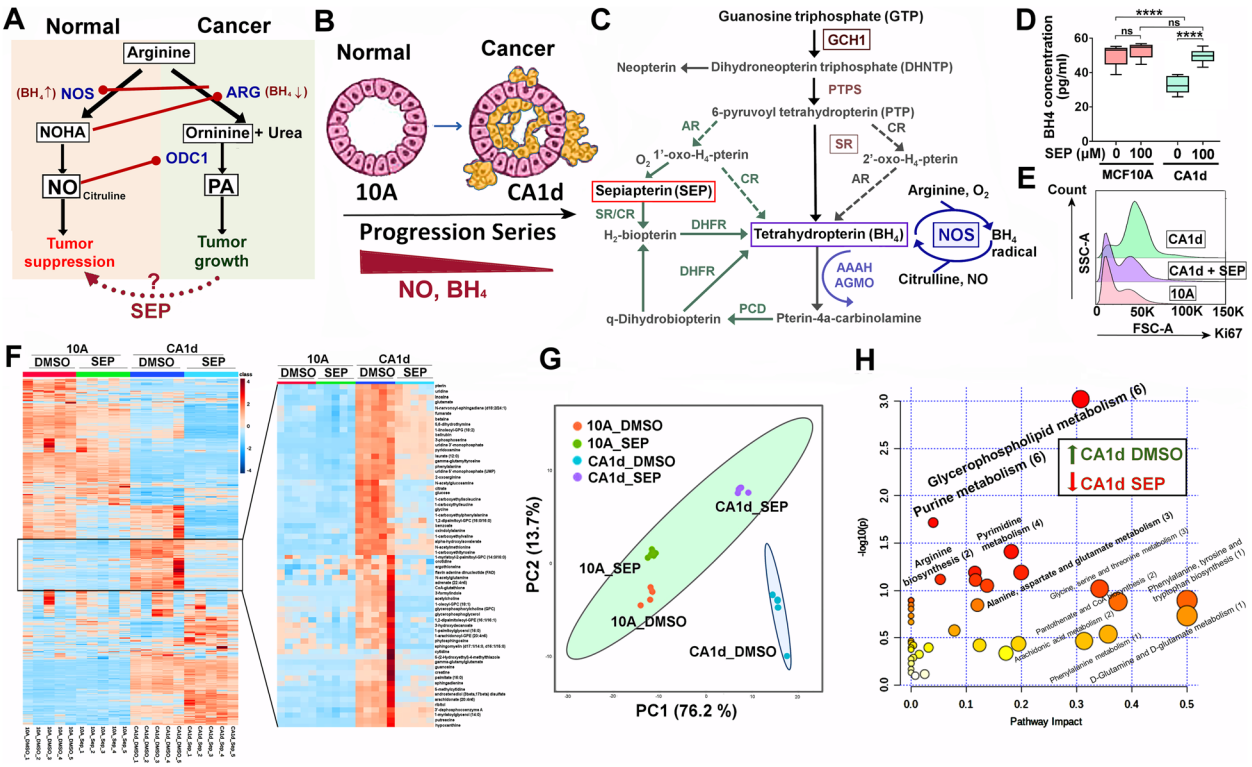

Fig. 1 Reprogramming arginine metabolism inhibits the growth of HER2 + breast cancer cells. **A** Bimodal arginine metabolism leading to two antagonizing pathways: NO vs. PA syntheses. NOS: nitric oxide synthase, NOHA (Nω-hydroxy-nor-arginine); ARG: arginase; ODC1: ornithine decarboxylase 1. **B** MCF10A (normal) CA1d (invasive) progression in MCF10A human breast cancer progression series showing the decrease of NO and BH_4 levels along with cancer progression. **C** BH_4 biosynthesis pathways featuring sepiapterin (SEP) as a precursor. **D** BH_4 levels in cancerous CA1d compared to normal MCF10A cells determined by ELISA. Note the normalization of BH_4 levels in CA1d cells after SEP (100 μM) treatment for 2 days [12]. Error bars: ± SEM. ****, $p \leq 0.0001$ and ns, $p > 0.05$. **E** Levels of a proliferation marker Ki67 in CA1d cells treated with SEP analyzed by flow cytometry. **F** (Left) Heatmap of metabolite levels in MCF10A cells vs. CA1d cells with or without SEP treatment (100 μM) ($n = 5$). (Right) Metabolites normalized in CA1d cells after SEP treatment. **G** Principal component analysis (PCA) of metabolites normalized in SEP-treated CA1d cells. Note the co-localization of SEP-treated CA1d cells with 10A cells (DMSO or SEP-treated) and a segregation of DMSO-treated CA1d cells. **H** Pathway analysis of metabolites normalized (downmodulated) in SEP-treated CA1d cells. Note the significant involvements of fatty acid and nucleotide metabolisms in the normalized pathways

from those of control CA1d cells (Fig. 1F, G). These normalized metabolites largely belonged to fatty acid and nucleotide metabolisms involved in energy production (Fig. 1H) [40]. The results show that SEP induces reprogramming of arginine metabolism and other metabolic pathways to inhibit HER2 + breast cancer cell growth.

Redirecting arginine metabolism reprograms tumor-associated macrophages (TAMs)

HER2 + breast tumors have poor immunogenicity due to abundant immune-suppressive cells, including M2-TAMs [10, 41, 42]. TAMs consist of the immune-stimulatory, tumoricidal M1-type and immune-suppressive, pro-tumor M2-type, which could be recapitulated by specific cytokine treatment of macrophages in vitro (Fig. 2A). M1 vs. M2 TAM formation largely depends on differential arginine metabolism [18]. M1-TAMs convert arginine to NO for pro-inflammatory signaling, whereas M2-TAMs convert arginine to PAs for anti-inflammatory signaling (Fig. 2B) [18, 43]. By using human monocytic cell line THP-1, we demonstrated that inhibiting NO production in M1 macrophages with an NOS2 inhibitor 1400W lowered an M1 marker TNFα, while elevating an M2 marker CD206. Conversely, inhibiting PA production in M2 macrophages with an arginase inhibitor NOHA (Nω-hydroxy-nor-arginine) elevated TNFα, while downmodulating CD206 (Fig. 2C). Such differential arginine metabolism in M1 vs M2 TAMs is likewise attributed to the different BH_4 availability. We indeed found that M2 macrophages produced significantly lower levels of BH_4 than M1 macrophages. However, SEP treatment of M2 macrophages restored BH_4 levels similar to those of M1 macrophages (Fig. 2D). At the same time, SEP-treated M2 macrophages came to express an M1 marker TNFα, while downmodulating an M2 marker CD163 (Fig. 2E) [18, 19]. Consistently, SEP-treated M2 macrophages elevated an M1 cytokine IL-12 in a dose-dependent manner, while downmodulating M2 cytokine IL-10, further attesting to a phenotypic conversion of M2 to M1 macrophages (Fig. 2F). These observations were recapitulated in human PBMC-derived macrophages, where SEP-treated M2 macrophages elevated M1 markers CD40 and CD80, while downmodulating M2 markers CD206 and CD163 (Fig. 2G).

Further metabolomic analysis showed that, in addition to arginine metabolic pathways, SEP treatment also lowered a group of other metabolites in M2 macrophages to the levels of M1 type, greatly differentiating their levels from those of control M2 macrophages (Fig. 2H, I). Most such metabolites belonged to the pathways involved in energy production, including TCA cycle, lipid and amino acid metabolism (Fig. 2J). In particular, elevated TCA cycle and sphingolipid metabolism are the hallmarks of M2 macrophages [44, 45], and their reduction by SEP treatment indicates the conversion of M2 to M1 types. These results demonstrate that SEP induces reprogramming of arginine and other metabolic pathways in M2 macrophages and converts their phenotype to M1 type. In fact, we previously reported that these SEP-treated M2 macrophages are functionally reprogrammed to M1 macrophages and able to induce effector T cells to kill adjacent tumor cells [19].

(See figure on next page.)

Fig. 2 Redirecting arginine metabolism reprograms tumor-associated macrophages (TAMs). **A** Scheme for differentiation of monocytes into naïve (M0) macrophages and subsequent M1 vs. M2 polarization in vitro. **B** Discrete arginine metabolic pathways in M1 vs. M2 macrophages and their antagonistic relationships, also showing scheme for phenotypic conversions: M1 → M2 conversion by inhibiting NOS2 in M1; M2 → M1 conversion by inhibiting ARG1 or providing SEP to M2 [18, 19]. **C** (Top) Levels of M1 marker TNFα in THP-1-derived macrophage subsets (M0, M1, or M2) treated with an NOS2 inhibitor 1400W or an ARG1 inhibitor NOHA. MFI: Mean fluorescence intensity determined by flowcytometry. (Bottom) Levels of M2 marker CD206 in macrophage subsets treated with 1400W or NOHA. Note that 1400W treatment of M1 cells lowered TNFα levels, but elevated CD206 levels, indicating conversion of M1 to M2 types. Conversely, NOHA treatment of M2 cells elevated TNFα levels, but lowered CD206 levels, indicating conversion of M2 to M1 types. **D** BH_4 levels in THP-1-derived macrophage subsets with or without SEP treatment determined by ELISA. Note the dramatically low BH_4 levels in M2 macrophages and the dose-dependent increases after SEP treatment (50, 100, or 200 μM) for 3 days. **E** (Top) Western blot for the levels of M2 marker CD163 and M1 marker TNFα in THP-1-derived macrophage subsets with or without SEP treatment. Note that SEP treatment (50, 100, or 200 μM, but not 500 μM (due to reduced cell viability)) of M2 macrophages lowered CD163 levels, while elevating TNFα levels. (Bottom) Quantification of TNFα and CD163 intensities. **F** Levels of M1 marker IL-12 (left) and M2 marker IL-10 (right) in THP-1-derived macrophage subsets with or without SEP treatment determined by ELISA. **G** Percentages of M1 marker CD40-positive (top row) vs. M2 marker CD206-positive cells (bottom row) in human PBMC-derived macrophages (M0, M1, or M2) with or without SEP treatment (50, 100, or 200 μM) determined by flowcytometry. Error bars: ± SEM. *, $p \le 0.05$; **, $p \le 0.01$; ***, $p \le 0.001$; ****, $p \le 0.0001$ and ns, $p > 0.05$. **H** (Left) Heatmap of metabolite levels in THP-1-derived M1 vs. M2 macrophages treated with control DMSO vs. SEP (100 μM) ($n = 5$). (Right) Metabolites normalized in M2 macrophages after SEP treatment. **I** PCA of metabolites normalized in SEP-treated M2 macrophages. Note the co-localization of SEP-treated M2 with M1 macrophages (both DMSO and SEP-treated) and segregation of DMSO-treated M2 macrophages. **J** Pathway analysis of metabolites normalized (downmodulated) in SEP-treated M2 macrophages. Note the involvements of these metabolites in energy production, including TCA cycle, lipid and amino acid metabolism

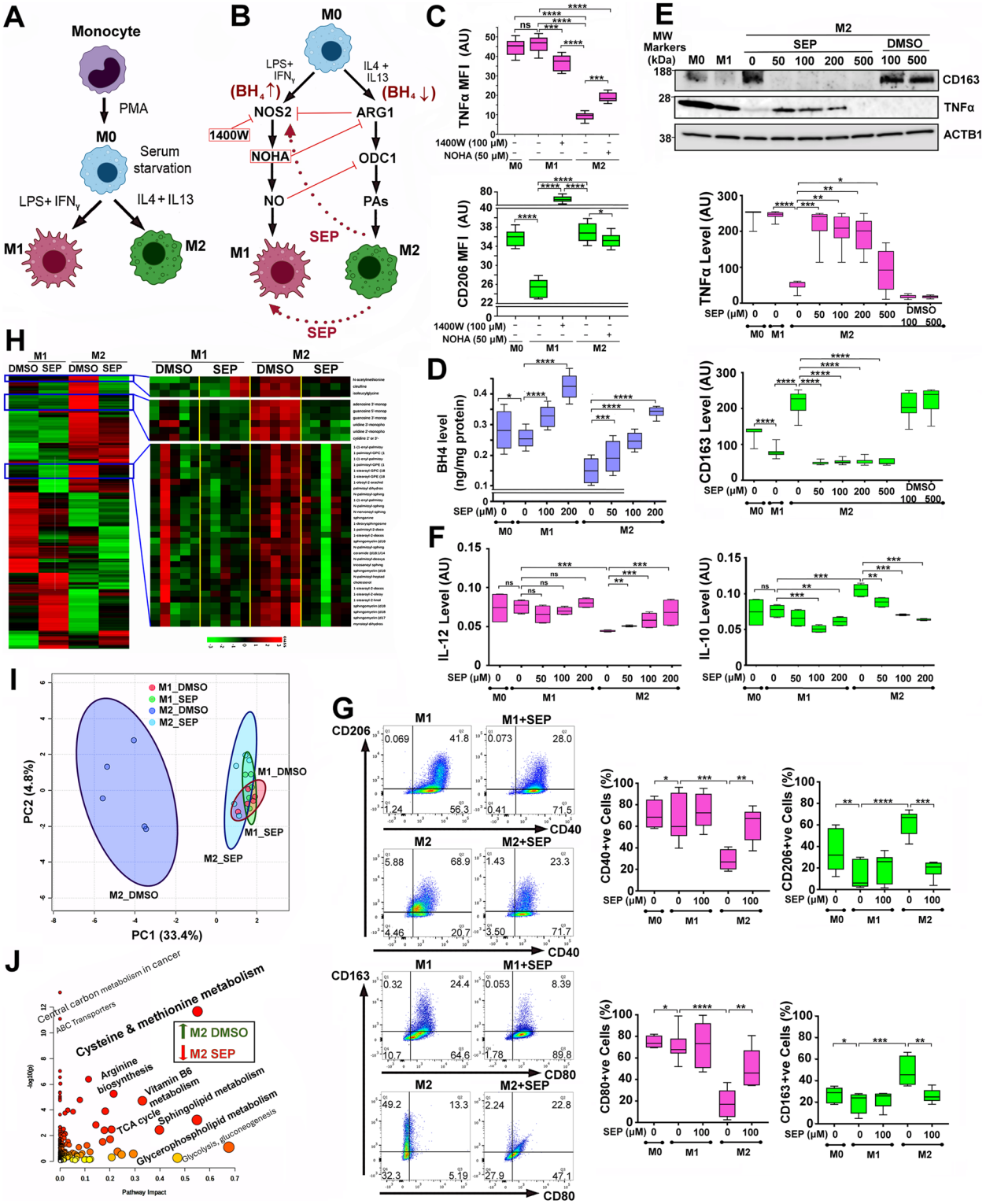

Fig. 2 (See legend on previous page.)

SEP treatment suppresses mammary tumor growth in MMTV-neu mice, while inducing systemic immunological reprogramming

The above results showed that SEP normalized the phenotypes of both breast cancer cells and TAMs. We then tested whether SEP could indeed suppress mammary tumor formation in vivo using MMTV-neu mice, a mouse model of spontaneous HER2-positive mammary tumors. These animals developed spontaneous single-focal mammary tumors at the latencies of 6–14 months [19]. Once tumors became palpable, animals were divided into the control (DMSO) vs. SEP (10 mg/kg) treatment groups ($n=7$/treatment) and given the drug through drinking water for 6 weeks, as we previously performed [19]. Tumor growth was measured twice a week using a caliper, and morbidity of animals were also observed. We saw almost 50% reduction of the tumor growth in the SEP-treated group without any morbidity of animals (Fig. 3A). Interestingly, SEP-treated tumors were more differentiated than DMSO-treated tumors and contained numerous mammary gland-like structures (Fig. 3B). To determine the immunogenicity of these tumors, we isolated TAMs and profiled their M1- vs. M2-TAM marker expression. In SEP-treated group, we saw significant increases of M1 markers (CD80 and IL12) but decreases of M2 markers (CD163 and IL10), whereas DMSO-treated group showed the opposite trends (Fig. 3C). Such an increase of M1-TAMs and decrease of M2-TAMs in SEP-treated tumors were expected to significantly contribute to the tumor inhibitory effects of the drug. We next tested whether a long-term treatment of SEP at a lower dosage could prevent mammary tumor incident in susceptible individuals. We treated MMTV-neu mice with SEP (1 mg/kg) vs. DMSO ($n=20$/treatment) via drinking water starting at their prepubertal stage (5 weeks old) and spanning 8 months. While 90% of DMSO-treated mice had developed tumors within 8 months, over 50% of SEP-treated mice were completely protected from tumor occurrence (Fig. 3D).

To explore the mechanism of such strong tumor-suppressive effects of SEP, we performed single cell sequencing analysis on PBMCs of MMTV-neu mice after 8 months of treatment with DMSO vs. SEP. These animals were divided into 4 groups: 1) DMSO with tumors (90% DMSO mice); 2) DMSO without tumors (10% DMSO mice); 3) SEP without tumors (55% SEP mice); and 4) SEP with tumors (45% SEP mice) (Fig. 3E). Isolated PBMCs were analyzed by single cell sequencing. Cell type analysis showed that PBMCs of SEP without tumor group were mainly T cells (CD8 + and CD4 +) and NK cells, whereas those of DMSO without tumor group were mostly B lymphocytes, attesting to the general anti-tumor roles of lymphocytes [46]. Conversely, PBMCs of SEP with tumor group were mostly macrophages, whereas those of DMSO with tumor group were largely granulocytes, especially, neutrophils, attesting to pro-tumor roles of myeloid cells (Fig. 3E) [47]. For further analyses, we focused on comparisons between SEP without tumor vs. DMSO with tumor groups, which were the major subgroups of the animals. Differentially expressed gene set analysis showed that PBMCs of SEP without tumor group had increased expression of a number of pro-immunogenic genes involved in T /NK cell functions (TNFAP3, PIM1, LMO2, ATF3, CD69, CD74, IF130, TCF4, and MEF2C) [48–56]. Conversely, these PBMCs showed decreased expression of a list of immune suppressive genes (S100A8/9, MMP9, TGFB1, LILR4B, LILRB4A, CCR1, HP, CSF3R, and SOCS1) (Fig. 3F, G) [57–64]. These results demonstrate that SEP exerts potent suppressive effects on HER2-positive mammary tumors and such anti-tumor effects are linked to the systemic immunological reprogramming to elevate anti-tumor lymphocytes.

(See figure on next page.)

Fig. 3 SEP treatment suppresses mammary tumor growth of MMTV-neu mice, while inducing systemic immunological reprogramming. **A** Tumor growth of MMTV-neu (unactivated) mice treated with control DMSO vs. SEP (10 mg/kg) ($n=7$). MMTV-neu mice were allowed to develop palpable mammary tumors and given DMSO or SEP in drinking water for 6 weeks. Tumors were measured by caliper and the volume was determined (V = (W(2) x L)/2). **B** Eosin & hematoxylin-stained tumor sections captured with 10 × or 40 × objectives. Note the presence of numerous mammary gland-like structures in SEP-treated tumors, but not in DMSO-treated tumors. Scale bars: 50 µm. **C** Percentages of M1 marker (CD80 or IL12)-positive TAMs vs. M2 marker (CD163 or IL10)-positive TAMs in DMSO vs. SEP-treated tumors determined by flow cytometry. Error bars: ± SEM. *, $p \le 0.05$; ****, $p \le 0.0001$. **D** Tumor-free survival curves of MMTV-neu mice treated with control DMSO vs. SEP (1 mg/kg, $n=20$). MMTV-neu mice were treated with DMSO vs. SEP starting at the age of 4 weeks and spanning over 7 months. **E** Major cell types (top) and sub cell types (middle) of PBMCs of different subgroups of MMTV-neu mice (DMSO with tumor, DMSO without tumor, SEP with tumor, and SEP without tumor groups) determined by single cell sequencing. (Bottom) UMAPs featuring the major cell type for each group. Note the enrichment of T cells in PBMCs of SEP without tumor group. **F** Volcano plot for differentially expressed genes in PBMCs of MMTV-neu mice which were SEP-treated and did not develop tumors (SEP without tumors) vs. DMSO-treated and developed tumors (DMSO with tumors). **G** Chord diagrams of genes elevated (left) or downmodulated (right) in PBMCs of SEP without tumor group compared to those of DMSO with tumor group

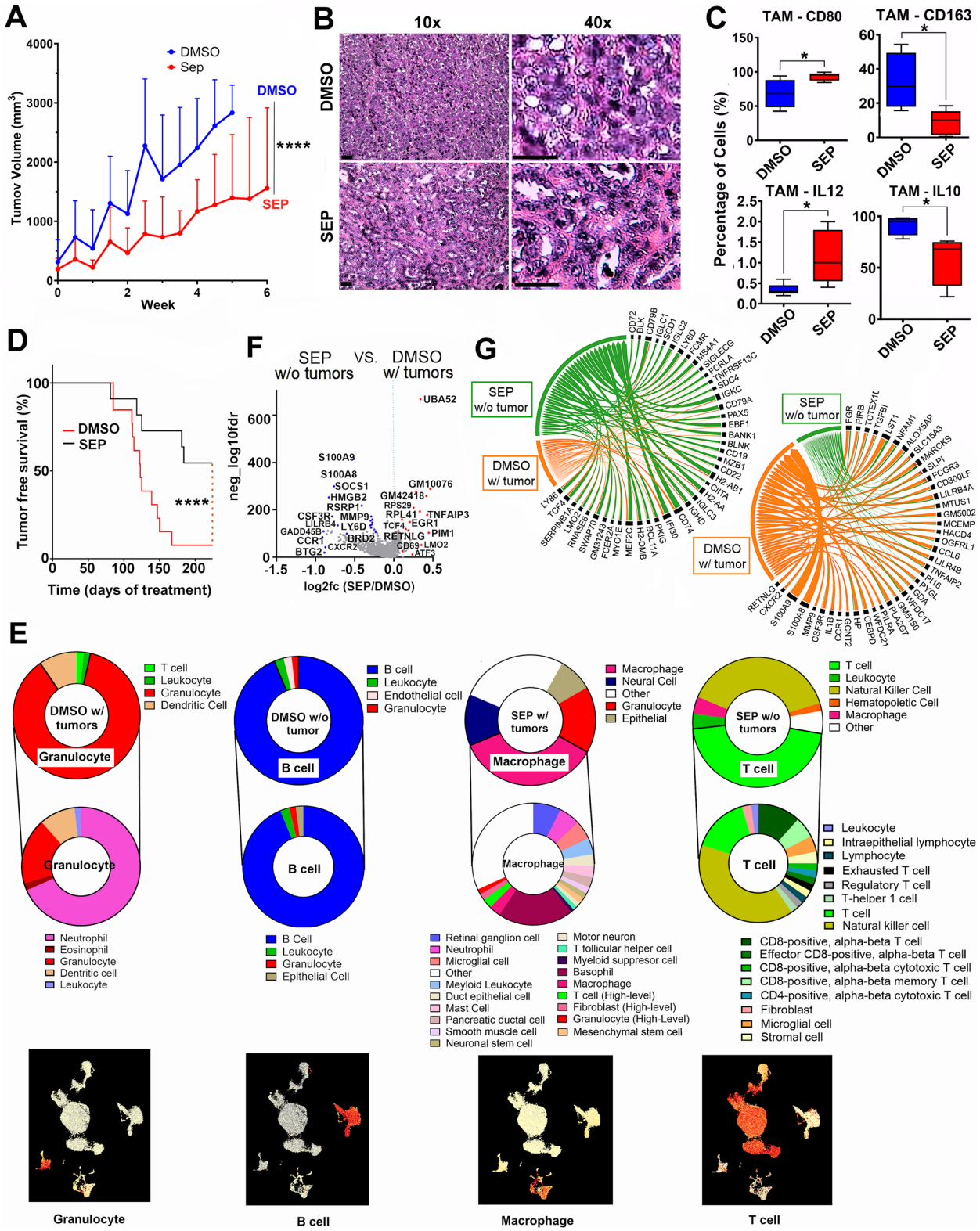

Fig. 3 (See legend on previous page.)

Long-term SEP treatment induces systemic metabolic reprogramming in MMTV-neu mice

To examine the potential causes for the different immunological landscapes between SEP-treated (no tumor) and DMSO-treated (with tumor) groups, we compared their systemic metabolic profiles by analyzing their plasma metabolites. We saw global decreases of metabolites in the SEP-treated group compared to the DMSO-treated group (Fig. 4A). Analysis of differentially represented metabolites revealed that those downmodulated in the SEP-treated group mostly belonged to energy production and immune suppression pathways, including

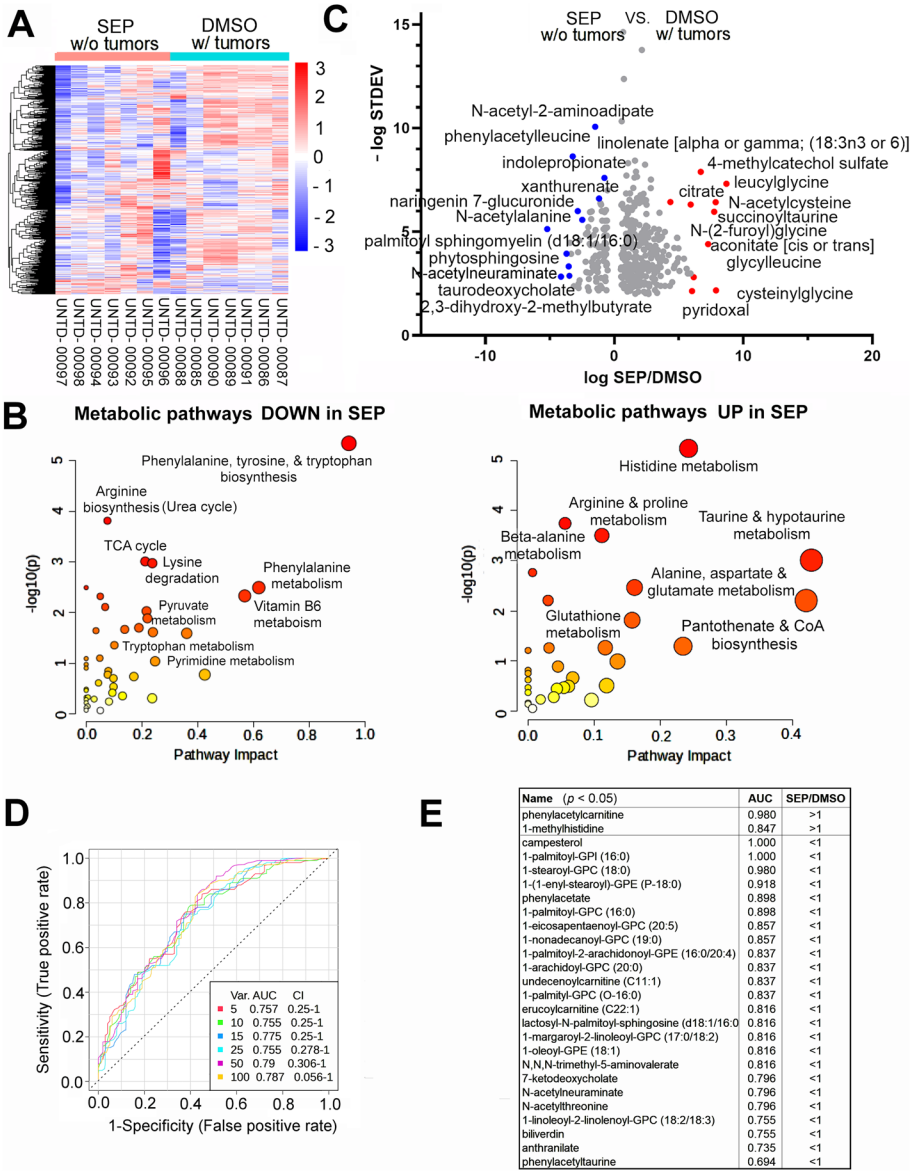

E

Name ($p < 0.05$)	AUC	SEP/DMSO
phenylacetylcarnitine	0.980	>1
1-methylhistidine	0.847	>1
campesterol	1.000	<1
1-palmitoyl-GPI (16:0)	1.000	<1
1-stearoyl-GPC (18:0)	0.980	<1
1-(1-enyl-stearoyl)-GPE (P-18:0)	0.918	<1
phenylacetate	0.898	<1
1-palmitoyl-GPC (16:0)	0.898	<1
1-eicosapentaenoyl-GPC (20:5)	0.857	<1
1-nonadecanoyl-GPC (19:0)	0.857	<1
1-palmitoyl-2-arachidonoyl-GPE (16:0/20:4)	0.837	<1
1-arachidoyl-GPC (20:0)	0.837	<1
undecenoylcarnitine (C11:1)	0.837	<1
1-palmityl-GPC (O-16:0)	0.837	<1
erucoylcarnitine (C22:1)	0.816	<1
lactosyl-N-palmitoyl-sphingosine (d18:1/16:0	0.816	<1
1-margaroyl-2-linoleoyl-GPC (17:0/18:2)	0.816	<1
1-oleoyl-GPE (18:1)	0.816	<1
N,N,N-trimethyl-5-aminovalerate	0.816	<1
7-ketodeoxycholate	0.796	<1
N-acetylneuraminate	0.796	<1
N-acetylthreonine	0.796	<1
1-linoleoyl-2-linolenoyl-GPC (18:2/18:3)	0.755	<1
biliverdin	0.755	<1
anthranilate	0.735	<1
phenylacetyltaurine	0.694	<1

Fig. 4 Long-term oral SEP induces systemic metabolic reprogramming in MMTV-neu mice. **A** Heatmap of metabolite levels in the plasma of SEP without tumor group vs. DMSO with tumor group of MMTV-neu mice ($n = 7$). Note the global decreases of metabolites in SEP without tumor group. **B** Metabolic pathways downregulated (left) and upregulated (right) in SEP without tumor group compared to DMSO with tumor group. Note that metabolites lowered in the former group mostly belonged to energy production and immune suppression pathways, including TCA cycle, nucleotide, phenylalanine, and tryptophan metabolism. Conversely, metabolites elevated in the former group mainly belonged to pro-inflammatory pathways, including histidine/histamine, taurine, and CoA metabolism. **C** Volcano plot for differentially represented metabolites in the plasma of SEP without tumor group vs. DMSO with tumor group. Note the significant reduction of tumor-associated metabolites, including N-acetylneuraminate and palmotyl sphingomyelin [70, 84]. Conversely, the increases in citrate and aconitate indicate inhibition of the TCA cycle. **D** Receiver operating characteristic (ROC) curve analysis (multivariate, random forest regression) on differentially represented metabolites. **E** Metabolites with the largest Area under Curve values (AUC ~ 1) and statistical significance ($p < 0.05$)

TCA cycle, nucleotide, phenylalanine, and tryptophan metabolism (Fig. 4B) [65–67]. Such metabolites downmodulated in the SEP-treated group included N-acetylneuraminate, N-acetylalanine, and taurodeoxycholate (Fig. 4C) involved in immunosuppression/exhaustion as well as carcinogenesis [68–73]. Conversely, metabolites upregulated in SEP-treated group mainly belonged to pro-inflammatory pathways, including histidine/histamine, taurine, and CoA metabolism (Fig. 4B) [74–76]. Those metabolites elevated in the SEP-treated group included linolenate (α and γ), S-acetylcysteine, citrate, and succinoyltaurine (Fig. 4C), involved in immune activation and tumor suppression [77–83].

To determine potential biomarkers, we analyzed Receiver Operating Characteristic (ROC) curves (multivariate, random forest regression) (Fig. 4D). The analysis identified a list of metabolites differentially represented in SEP-treated vs. DMSO-treated groups with the highest accuracy (i.e., Area under Curve values (AUC) ~ 1). Metabolites with the highest accuracy (AUC = 1.0–0.98) were campesterol, 1-palmitoyl-glycerophosphoinositol (GPI)(LysoPI), and 1-stearoyl-GPC (LycoPC) which were all involved in immunosuppression [85–87] and downmodulated in SEP-treated group (Fig. 4E). Conversely, the metabolite elevated in SEP-treated group with the highest accuracy (AUC = 0.98) was phenylacetylcarnitine produced by gut microbial metabolism (Fig. 4E) [88, 89], indicating SEP's ability to reprogram the metabolism of gut microbiota in addition to the host. Another metabolite elevated in SEP-treated group with high accuracy (AUC = 0.847) was 1-methylhistidine, which is a marker for muscle turnover during extensive exercise and is also an antioxidant [90, 91]. This could be due to high levels of NO production after SEP treatment promoting muscle development and functions [92]. These results altogether demonstrate that SEP-treatment induced systemic metabolic reprogramming to promote immunological responses.

Bone marrow of SEP-treated MMTV-neu mice has increased levels of total T cells

To further examine the systemic immunological reprogramming by SEP treatment, we determined the epigenetic profiles of the bone marrows (BM) of drug-treated mice by CUT&Tag analysis for H3K27me3 (suppression) and H3K27ac (activation) histone marks. The heatmaps and peak sizes of the epigenome showed that both histone marks were higher in SEP without tumor group than DMSO with tumor group (Fig. 5A, B). A list of genes with elevated H3K27me3 marks (more strongly suppressed) after SEP treatment mostly belonged to pathways involved in immune suppression (e.g., lymphocyte apoptosis and IL5 production) (Fig. 5C, left) [93]. Conversely, a gene set with elevated H3K27ac mark (more strongly activated) after SEP treatment largely belonged to pathways involved in pro-inflammatory responses (e.g., leukocyte activation and IL-6 production)(Fig. 5C, right) [94]. Such SEP-activated genes included those involved in T cell activation and development (IL6RA, IL7R, IFNGR2, and CD44) [95–98], indicating that SEP might have epigenetically induced T cell development (Fig. 5D). To confirm this observation, we analyzed the cellular components of the BM of SEP- vs. DMSO-treated groups based on their epigenetic patterns of the genome. We found that the BM of SEP-treated group contained significantly higher total counts of T cells, B cells, and stem cells than DMSO-treated group (Fig. 5E). Interestingly, BM-resident T cells are mostly memory T cells returning from distant tissues/organs [20–22], unlike B cells which undergo most of the maturation in the BM [99]. Thus, in addition to enhanced lymphogenesis, as indicated by the increases in B cell and stem cell counts, SEP treatment possibly promoted formation of memory T cells to exert long-term protection against tumor formation [100]. In fact, certain memory T cell markers, namely, IL6RA, IL7R, IFNGR2, and CD44 [20, 95–98, 101], were highly elevated by SEP treatment (Fig. 5D), further supporting the possibility of enhanced memory T cell formation by a long-term SEP treatment. Our results altogether strongly suggest that SEP might be utilized as a novel immunotherapeutic agent for preventing HER2-positive breast cancer.

Discussion

Recent studies have unveiled dynamic and reciprocal interactions between metabolism and immunity in the body [102]. A variety of metabolic signaling pathways not only drive the development of immune cells, but also determine the immunogenicity of tissues/organs and the rest of the body. Conversely, different immunological responses, represented by the expression of unique transcription factors and distinct cytokines, drive cognate metabolic pathways. For example, T helper 1 (Th1) cells (expressing T-bet and IFN-γ) signal to promote glycolysis in macrophages, while downmodulating tricarboxylic acid (TCA) cycle, fatty acid oxidation, and glutaminolysis, inducing their polarization to the pro-inflammatory M1-type. Promotion of glycolysis for energy production is beneficial to M1 TAMs, since they are mostly localized in hypoxic environments that inherently trigger glycolysis [103]. In contrast, Th2 cells (expressing GATA3, IL-4, and IL-13) signal to activate peroxisome proliferator-activated receptor gamma (PPARγ) in macrophages to promote lipid metabolism (e.g., fatty acid uptake/oxidation) as well as mitochondrial biogenesis/respiration, inducing their polarization

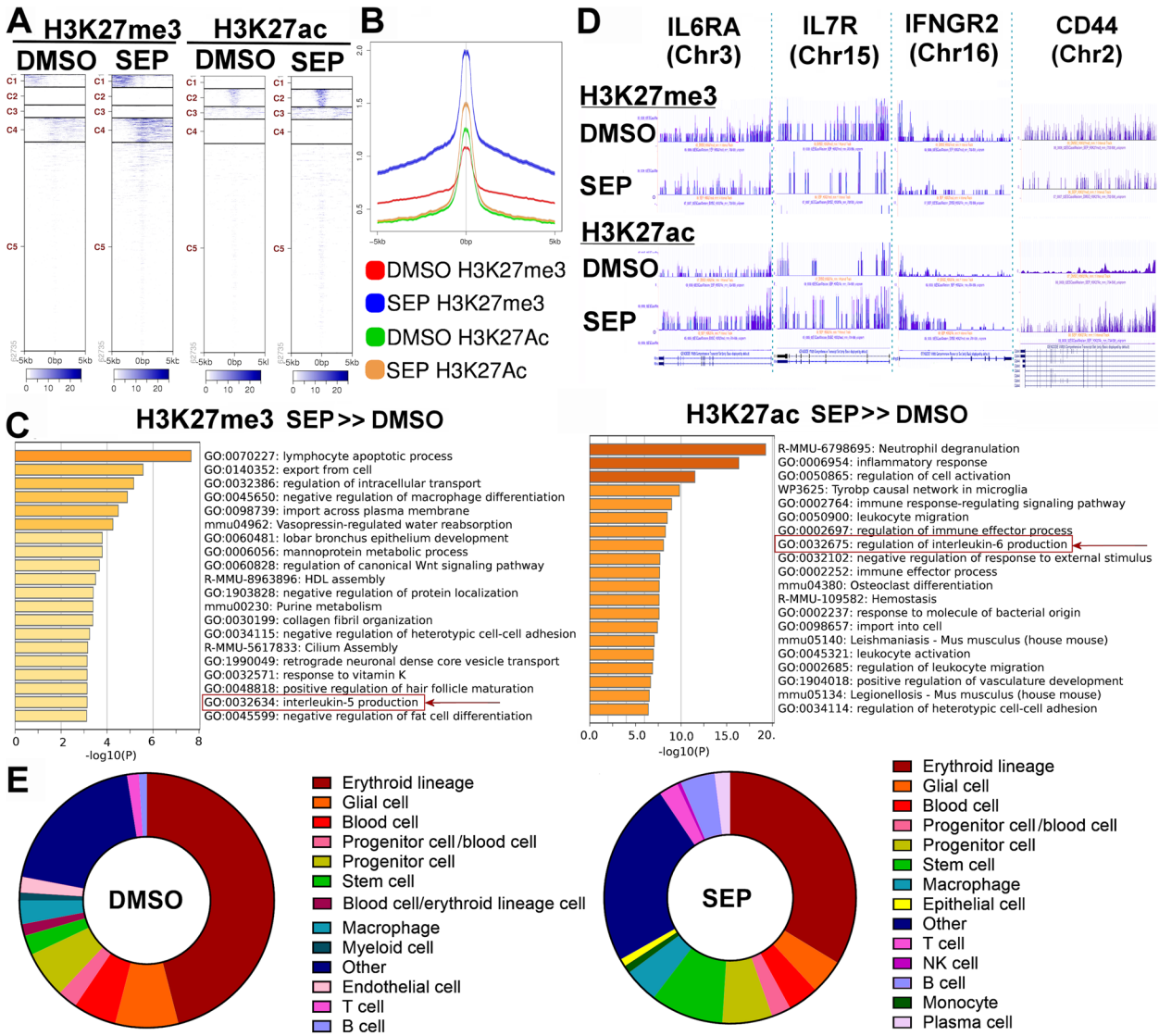

Fig. 5 CUT & Tag analysis of bone marrow of SEP-treated MMTV-neu mice reveals increased levels of total T cells. **A-B** The heatmaps (**A**) and peak sizes (**B**) of H3K27me3 (suppression) and H3K27ac (activation) histone marks of the bone marrows of DMSO with tumor vs. SEP without tumor groups of MMTV-neu mice. Note that both histone marks were higher in the latter than the former groups. **C** Pathways of genes with elevated H3K27me3 mark (more strongly suppressed, left) vs. pathways of genes with elevated H3K27ac mark (more strongly activated, right) in SEP without tumor group compared to DMSO with tumor group. Note that SEP-suppressed pathways belonged to those involved in immune suppression (e.g., IL5 production), whereas SEP-activated pathways belonged to those involved in pro-inflammatory responses (e.g., IL-6 production). **D** H3K27me3 and H3K27ac marks of select SEP-activated genes involved in T cell activation or memory T cell formation (IL6RA, IL7R, IFNGR2, and CD44 [95–98]. **E** Bone marrow cell compositions determined based on epigenomic profiles (predicted by Cellkb). Note the significant increase in T cell, NK cell and stem cells in the bone marrow of SEP-treated animals

to the anti-inflammatory M2-type [102]. Promotion of mitochondrial respiration and fatty acid oxidation for energy production is beneficial to M2-TAMs, since they usually do not have enough glucose supply for glycolysis after its rapid consumption by tumor cells [103]. Furthermore, recent studies demonstrated the critical roles of distinct arginine metabolic pathways, namely, NO vs. PAs, in formation and functions of M1- vs. M2-macrophages, respectively [8, 19, 104, 105]. Arginine metabolic pathways are also found to play essential roles in regulation of T cell activities. For example, NO promotes T cell proliferation/activation, while elevating the Th1/Th2 ratios [106]. Conversely, PAs, elevated in response to T cell activation, help determine T helper cell lineages (Th1, Th2, Th17, and Treg), while inhibiting memory T cell formation [7, 107].

Such close linkages between metabolic pathways and immune responses have led to the recent emergence of the concept of Immunometabolism [108, 109]. A number of metabolic modulators have been developed aiming to target certain metabolic pathways for cancer therapy [110]. One of the most explored metabolic pathways is arginine. In cancer, arginine tends to be converted to protumor PAs due to downmodulation of NO synthesis under reduced availability of the NOS cofactor BH_4 [11, 18, 19]. Different strategies have been explored seeking to normalize arginine metabolism in cancer, where most such efforts have been focused on arginine deprivation therapy and PA synthesis inhibitors [6, 13, 14, 110]. Although these approaches have shown some therapeutic benefits, their reported serious adverse side effects (e.g., hearing loss and hematologic disorders) limit their usability [15, 16].

In our previous studies, we showed that SEP, the endogenous BH_4 precursor, could correct arginine metabolism in animal models of HER2-positive mammary tumors. We saw that supplementing SEP induced metabolic and phenotypic reprogramming of tumor cells as well as TAMs and effectively inhibited HER2-positive mammary tumor growth [18, 19]. Besides, SEP has no dose-limiting toxicity reported during the Phase I trial for phenylketonuria treatment [17]. In the present study, we tested the effects of a long-term use of SEP on tumor prevention. We reported that a long-term oral administration of SEP to animals prone to HER2-positive mammary tumors strongly prevented tumor occurrence for 8 months, while most control animals had developed tumors. These SEP-treated animals had undergone the reprogramming of the systemic metabolism and immunity, elevating total T cell counts in the circulation and bone marrow. Given that bone marrow-resident T cells are mostly memory T cells [20–22], it is possible that SEP promoted memory T cell formation, leading to potent tumor prevention. These findings suggest the possible roles of the SEP/BH_4/NO axis in promoting memory T cell formation, at least in part, by inhibiting PA synthesis known to inhibit CD8+memory T cell formation [7]. Since therapeutic approaches to elevate memory T cells have been yet at the early developmental stages, clinical uses of the SEP/BH_4 pathway for cancer prevention would warrant further investigation.

Supplementary Information

The online version contains supplementary material available at https://doi.org/10.1186/s40170-025-00384-4.

Supplementary Material 1.

Supplementary Material 2.

Supplementary Material 3.

Supplementary Material 4.

Acknowledgements

We thank Raghvendra Srivastava, Vladimirand Makarov, and Ivan Juric of the Discovery Lab in the Global Center for Immunotherapy and Precision Immuno-Oncology at Cleveland Clinics Foundation for single-cell sequencing and analysis. We would also like to thank the research teams at Metabolon, Inc. for metabolomic analyses; Active Motif for CUT&Tag analysis; and Drs. Andrea Kalinoski and David Weaver in the Imaging Core at the University of Toledo for various support in FACS analyses.

Authors' contributions

Conceptualization, V.S, V.F., and S.F; Methodology, V.S, V.F, X.Z., E.C., V.T., O.S., and S.F; Formal Analysis: V.S, V.F, and S.F.; Investigation, V.S., V.F, X.Z., E.C., and V.T.; Data Curation, V.S, V.F. and S.F; Writing – Original Draft Preparation, S.F.; Revision-V.T., J.S., and S.F.; Visualization, V.S, V.F and S.F.; Supervision, S.F.; Project Administration, S.F.; Funding Acquisition, S.F.

Funding

This work was supported by the startup fund from the University of Toledo Health Science Campus, College of Medicine and Life Sciences, Department of Cancer Biology to S.F; Ohio Cancer Re-search Grant (Project #: 5017) to S.F; Medical Research Society (Toledo Foundation, #206298) Award to S.F; American Cancer Society Research Scholar Grant (RSG-18–238-01-CSM) to S.F; and National Cancer Institute Research Grant (R01CA248304) to SF.

Data availability

No datasets were generated or analysed during the current study.

Declarations

Competing interests

The authors declare no competing interests.

Author details

[1]Department of Cell & Cancer Biology, College of Medicine and Life Sciences, University of Toledo Health Science Campus, 3000 Arlington Ave., Toledo, OH 43614, USA. [2]Department of Zoology and Physiology, University of Wyoming, 1000 E. University Ave, Biological Science Building, Room 319F, Laramie, WY 82071, USA. [3]Division of Rheumatology, University of Colorado, Anschutz Medical Campus Barbara Davis Center, Mail Stop B115, 1775 Aurora Court, Aurora, CO 80045, USA. [4]MetroHealth Medical Center, Case Western Reserve University School of Medicine, Case Comprehensive Cancer Center, 2500 MetroHealth Drive, Cleveland, OH 44109, USA.

Received: 4 November 2024 Accepted: 7 March 2025
Published online: 20 March 2025

References

1. Tapiero H, Mathé G, Couvreur P, Tew KD. I. Arginine. Biomed Pharmacother. 2002;56(9):439–45.
2. Hogarty MD, Norris MD, Davis K, Liu X, Evageliou NF, Hayes CS, Pawel B, Guo R, Zhao H, Sekyere E, et al. ODC1 is a critical determinant of MYCN oncogenesis and a therapeutic target in neuroblastoma. Cancer Res. 2008;68(23):9735–45.
3. Bachmann AS, Geerts D. Polyamine synthesis as a target of MYC oncogenes. J Biol Chem. 2018;293(48):18757–69.
4. Bauer PM, Buga GM, Fukuto JM, Pegg AE, Ignarro LJ. Nitric oxide inhibits ornithine decarboxylase via S-nitrosylation of cysteine 360 in the active site of the enzyme. J Biol Chem. 2001;276(37):34458–64.
5. Tenu JP, Lepoivre M, Moali C, Brollo M, Mansuy D, Boucher JL. Effects of the new arginase inhibitor N(omega)-hydroxy-nor-L-arginine on NO synthase activity in murine macrophages. Nitric Oxide. 1999;3(6):427–38.
6. Thomas T, Thomas TJ. Polyamine metabolism and cancer. J Cell Mol Med. 2003;7(2):113–26.
7. Elmarsafawi AG, Hesterberg RS, Fernandez MR, Yang C, Darville LN, Liu M, Koomen JM, Ot Phanstiel, Atkins R, Mullinax JE, et al. Modulating the polyamine/hypusine axis controls generation of CD8+ tissue-resident memory T cells. JCI Insight. 2023;8(18):e169308.

8. Rath M, Müller I, Kropf P, Closs EI, Munder M. Metabolism via arginase or nitric oxide synthase: two competing arginine pathways in macrophages. Front Immunol. 2014;5:532.
9. Martinez FO, Gordon S, Locati M, Mantovani A. Transcriptional profiling of the human monocyte-to-macrophage differentiation and polarization: new molecules and patterns of gene expression. J Immunol. 2006;177(10):7303–11.
10. Biswas SK, Mantovani A. Macrophage plasticity and interaction with lymphocyte subsets: cancer as a paradigm. Nat Immunol. 2010;11(10):889–96.
11. Landmesser U, Dikalov S, Price SR, McCann L, Fukai T, Holland SM, Mitch WE, Harrison DG. Oxidation of tetrahydrobiopterin leads to uncoupling of endothelial cell nitric oxide synthase in hypertension. J Clin Invest. 2003;111(8):1201–9.
12. Ren G, Zheng X, Bommarito M, Metzger S, Letson J, Walia Y, Furuta S. Reduced basal nitric oxide production induces precancerous mammary lesions via ERBB2 and TGFβ. Sci Rep. 2019;9(1):6688.
13. Hayes CS, Shicora AC, Keough MP, Snook AE, Burns MR, Gilmour SK. Polyamine-blocking therapy reverses immunosuppression in the tumor microenvironment. Cancer Immunol Res. 2014;2(3):274–85.
14. Alexander ET, Minton A, Peters MC, OT Phanstiel, Gilmour SK. A novel polyamine blockade therapy activates an anti-tumor immune response. Oncotarget. 2017;8(48):84140–52.
15. Meyskens FL, Kingsley EM, Glattke T, Loescher L, Booth A. A phase II study of alpha-difluoromethylornithine (DFMO) for the treatment of metastatic melanoma. Invest New Drugs. 1986;4(3):257–62.
16. Tomlinson BK, Thomson JA, Bomalaski JS, Diaz M, Akande T, Mahaffey N, Li T, Dutia MP, Kelly K, Gong IY, et al. Phase I trial of arginine deprivation therapy with ADI-PEG 20 plus docetaxel in patients with advanced malignant solid tumors. Clin Cancer Res. 2015;21(11):2480–6.
17. Smith N, Longo N, Levert K, Hyland K, Blau N. Phase I clinical evaluation of CNSA-001 (sepiapterin), a novel pharmacological treatment for phenylketonuria and tetrahydrobiopterin deficiencies, in healthy volunteers. Mol Genet Metab. 2019;126(4):406–12.
18. Zheng X, Fernando V, Sharma V, Walia Y, Letson J, Furuta S. Correction of arginine metabolism with sepiapterin-the precursor of nitric oxide synthase cofactor BH(4)-induces immunostimulatory-shift of breast cancer. Biochem Pharmacol. 2020;176:113887.
19. Fernando V, Zheng X, Sharma V, Sweef O, Choi ES, Furuta S. Reprogramming of breast tumor-associated macrophages with modulation of arginine metabolism. Life Sci Alliance. 2024;7(11):e202302339.
20. Mazo IB, Honczarenko M, Leung H, Cavanagh LL, Bonasio R, Weninger W, Engelke K, Xia L, McEver RP, Koni PA, et al. Bone marrow is a major reservoir and site of recruitment for central memory CD8+ T cells. Immunity. 2005;22(2):259–70.
21. Lamble AJ, Kosaka Y, Laderas T, Maffit A, Kaempf A, Brady LK, Wang W, Long N, Saultz JN, Mori M, et al. Reversible suppression of T cell function in the bone marrow microenvironment of acute myeloid leukemia. Proc Natl Acad Sci U S A. 2020;117(25):14331–41.
22. Okhrimenko A, Grün JR, Westendorf K, Fang Z, Reinke S, von Roth P, Wassilew G, Kühl AA, Kudernatsch R, Demski S, et al. Human memory T cells from the bone marrow are resting and maintain long-lasting systemic memory. Proc Natl Acad Sci U S A. 2014;111(25):9229–34.
23. Debnath J, Muthuswamy SK, Brugge JS. Morphogenesis and oncogenesis of MCF-10A mammary epithelial acini grown in three-dimensional basement membrane cultures. Methods. 2003;30(3):256–68.
24. Pannirselvam M, Simon V, Verma S, Anderson T, Triggle CR. Chronic oral supplementation with sepiapterin prevents endothelial dysfunction and oxidative stress in small mesenteric arteries from diabetic (db/db) mice. Br J Pharmacol. 2003;140(4):701–6.
25. Yoshioka K, Otani H, Shimazu T, Fujita M, Iwasaka T, Shiojima I. Sepiapterin prevents left ventricular hypertrophy and dilatory remodeling induced by pressure overload in rats. Am J Physiol Heart Circ Physiol. 2015;309(10):H1782-1791.
26. Rabender CS, Alam A, Sundaresan G, Cardnell RJ, Yakovlev VA, Mukhopadhyay ND, Graves P, Zweit J, Mikkelsen RB: The role of nitric oxide synthase uncoupling in tumor progression. 2015(1557-3125 (Electronic)).
27. Krneta T, Gillgrass A, Chew M, Ashkar AA. The breast tumor microenvironment alters the phenotype and function of natural killer cells. Cell Mol Immunol. 2016;13(5):628–39.
28. Cassetta L, Noy R, Swierczak A, Sugano G, Smith H, Wiechmann L, Pollard JW. Isolation of Mouse and Human Tumor-Associated Macrophages. Adv Exp Med Biol. 2016;899:211–29. https://doi.org/10.1007/978-3-319-26666-4_12.
29. Zheng GX, Terry JM, Belgrader P, Ryvkin P, Bent ZW, Wilson R, Ziraldo SB, Wheeler TD, McDermott GP, Zhu J, et al. Massively parallel digital transcriptional profiling of single cells. Nat Commun. 2017;8:14049.
30. Hao Y, Hao S, Andersen-Nissen E, Mauck WM 3rd, Zheng S, Butler A, Lee MJ, Wilk AJ, Darby C, Zager M, et al. Integrated analysis of multimodal single-cell data. Cell. 2021;184(13):3573-3587.e3529.
31. Le TQ, Phan T, Pham MT, Tran DQ, Lam L, Nguyen T, et al. BBrowser: Making single-cell data easily accessible. 2020. bioRxiv.
32. Souza AL, Patti GJ. A Protocol for Untargeted Metabolomic Analysis: From Sample Preparation to Data Processing. Methods Mol Biol. 2021;2276:357–82.
33. Pang Z, Lu Y, Zhou G, Hui F, Xu L, Viau C, Spigelman Aliya F, MacDonald Patrick E, Wishart David S, Li S, et al. MetaboAnalyst 6.0: towards a unified platform for metabolomics data processing, analysis and interpretation. Nucleic Acids Research. 2024;52(W1):W398–406.
34. Yin Q, Li Y, Yin Y. CUT&Tag for efficient epigenomic profiling of frozen tissues. Methods Mol Biol. 2024;2846:181–9.
35. Li H, Durbin R. Fast and accurate short read alignment with Burrows-Wheeler transform. Bioinformatics. 2009;25(14):1754–60.
36. Love MI, Huber W, Anders S. Moderated estimation of fold change and dispersion for RNA-seq data with DESeq2. Genome Biol. 2014;15(12):550.
37. Lee SY, Meier R, Furuta S, Lenburg ME, Kenny PA, Xu R, Bissell MJ. FAM83A confers EGFR-TKI resistance in breast cancer cells and in mice. J Clin Invest. 2012;122(9):3211–20 PMCID: PMC3428077.
38. Furuta S, Ren G, Mao JH, Bissell MJ. Laminin signals initiate the reciprocal loop that informs breast-specific gene expression and homeostasis by activating NO, p53 and microRNAs. Elife. 2018;7:e26148 PMCID: PMC5862529.
39. McHugh ML. Multiple comparison analysis testing in ANOVA. Biochem Med (Zagreb). 2011;21(3):203–9.
40. Zhu J, Thompson CB. Metabolic regulation of cell growth and proliferation. Nat Rev Mol Cell Biol. 2019;20(7):436–50.
41. Decker T, Fischer G, Bücke W, Bücke P, Stotz F, Grüneberger A, Gropp-Meier M, Wiedemann G, Pfeiffer C, Peschel C, et al. Increased number of regulatory T cells (T-regs) in the peripheral blood of patients with Her-2/neu-positive early breast cancer. J Cancer Res Clin Oncol. 2012;138(11):1945–50.
42. Force J, Howie LJ, Abbott SE, Bentley R, Marcom PK, Kimmick G, Westbrook K, Sammons SL, Parks M, Topping DL, et al. Early stage HER2-positive breast cancers not achieving a pCR from neoadjuvant trastuzumab- or pertuzumab-based regimens have an immunosuppressive phenotype. Clin Breast Cancer. 2018;18(5):410–7.
43. Mills CD, Lenz LL, Ley K. Macrophages at the fork in the road to health or disease. Front Immunol. 2015;6:59.
44. Liu Y, Xu R, Gu H, Zhang E, Qu J, Cao W, Huang X, Yan H, He J, Cai Z. Metabolic reprogramming in macrophage responses. Biomark Res. 2021;9(1):1.
45. Morgan PK, Huynh K, Pernes G, Miotto PM, Mellett NA, Giles C, Meikle PJ, Murphy AJ, Lancaster GI. Macrophage polarization state affects lipid composition and the channeling of exogenous fatty acids into endogenous lipid pools. J Biol Chem. 2021;297(6):101341.
46. Yang YL, Yang F, Huang ZQ, Li YY, Shi HY, Sun Q, Ma Y, Wang Y, Zhang Y, Yang S, et al. T cells, NK cells, and tumor-associated macrophages in cancer immunotherapy and the current state of the art of drug delivery systems. Front Immunol. 2023;14:1199173.
47. Engblom C, Pfirschke C, Pittet MJ. The role of myeloid cells in cancer therapies. Nat Rev Cancer. 2016;16(7):447–62.
48. Matsuzawa Y, Oshima S, Takahara M, Maeyashiki C, Nemoto Y, Kobayashi M, Nibe Y, Nozaki K, Nagaishi T, Okamoto R, et al. TNFAIP3 promotes survival of CD4 T cells by restricting MTOR and promoting autophagy. Autophagy. 2015;11(7):1052–62.
49. Liu Z, Han M, Ding K, Fu R. The role of Pim kinase in immunomodulation. Am J Cancer Res. 2020;10(12):4085–97.
50. Hirano KI, Hosokawa H, Koizumi M, Endo Y, Yahata T, Ando K, Hozumi K. LMO2 is essential to maintain the ability of progenitors to differentiate into T-cell lineage in mice. Elife. 2021;10:e68227.

51. Ku HC, Cheng CF. Master regulator Activating Transcription Factor 3 (ATF3) in metabolic homeostasis and cancer. Front Endocrinol (Lausanne). 2020;11:556.
52. Cibrián D, Sánchez-Madrid F. CD69: from activation marker to metabolic gatekeeper. Eur J Immunol. 2017;47(6):946–53.
53. Zhang L, Woltering I, Holzner M, Brandhofer M, Schaefer C-C, Bushati G, Ebert S, Yang B, Muenchhoff M, Hellmuth JC, et al. CD74 is a functional MIF receptor on activated CD4+ T cells. Cell Mol Life Sci. 2024;81(1):296.
54. Nakamura T, Izumida M, Hans MB, Suzuki S, Takahashi K, Hayashi H, Ariyoshi K, Kubo Y. Post-transcriptional induction of the antiviral host factor GILT/IFI30 by interferon gamma. Int J Mol Sci. 2024;25(17):9663.
55. Angus-Hill ML, Elbert KM, Hidalgo J, Capecchi MR. T-cell factor 4 functions as a tumor suppressor whose disruption modulates colon cell proliferation and tumorigenesis. Proc Natl Acad Sci U S A. 2011;108(12):4914–9.
56. Li JH, Zhou A, Lee CD, Shah SN, Ji JH, Senthilkumar V, Padilla ET, Ball AB, Feng Q, Bustillos CG, et al. MEF2C regulates NK cell effector functions through control of lipid metabolism. Nat Immunol. 2024;25(5):778–89.
57. von Wulffen M, Luehrmann V, Robeck S, Russo A, Fischer-Riepe L, van den Bosch M, van Lent P, Loser K, Gabrilovich DI, Hermann S, et al. S100A8/A9-alarmin promotes local myeloid-derived suppressor cell activation restricting severe autoimmune arthritis. Cell Rep. 2023;42(8):113006.
58. Juric V, O'Sullivan C, Stefanutti E, Kovalenko M, Greenstein A, Barry-Hamilton V, Mikaelian I, Degenhardt J, Yue P, Smith V, et al. MMP-9 inhibition promotes anti-tumor immunity through disruption of biochemical and physical barriers to T-cell trafficking to tumors. PLoS ONE. 2018;13(11):e0207255.
59. Sharma N, Atolagbe OT, Ge Z, Allison JP. LILRB4 suppresses immunity in solid tumors and is a potential target for immunotherapy. J Exp Med. 2021;218(7):e20201811.
60. Li YL, Chen CH, Lai YS, Pan MR, Hung WC. Increased blood CSF3R(+) myeloid-derived suppressor cell is a predictor for breast cancer recurrence. Am J Cancer Res. 2024;14(6):3171–85.
61. Bidgood GM, Keating N, Doggett K, Nicholson SE. SOCS1 is a critical checkpoint in immune homeostasis, inflammation and tumor immunity. Front Immunol. 2024;15:1419951.
62. de Streel G, Lucas S. Targeting immunosuppression by TGF-β1 for cancer immunotherapy. Biochem Pharmacol. 2021;192:114697.
63. MacKellar M, Vigerust DJ. Role of haptoglobin in health and disease: a focus on diabetes. Clin Diabetes. 2016;34(3):148–57.
64. Le K, Sun J, Ghaemmaghami J, Smith MR, Ip WKE, Phillips T, Gupta M. Blockade of CCR1 induces a phenotypic shift in macrophages and triggers a favorable antilymphoma activity. Blood Adv. 2023;7(15):3952–67.
65. Mullen NJ, Singh PK. Nucleotide metabolism: a pan-cancer metabolic dependency. Nat Rev Cancer. 2023;23(5):275–94.
66. Zhang Q, Chen S, Guo Y, He F, Fu J, Ren W. Phenylalanine diminishes M1 macrophage inflammation. Sci China Life Sci. 2023;66(12):2862–76.
67. Seo SK, Kwon B. Immune regulation through tryptophan metabolism. Exp Mol Med. 2023;55(7):1371–9.
68. Lyu Q, Zhang L, Ding Y, Liu Z. Genetically predicted N-Acetyl-L-Alanine mediates the association between CD3 on activated and secreting Tregs and Guillain-Barre syndrome. Front Neurosci. 2024;18:1398653.
69. Suzzi S, Croese T, Ravid A, Gold O, Clark AR, Medina S, Kitsberg D, Adam M, Vernon KA, Kohnert E, et al. N-acetylneuraminic acid links immune exhaustion and accelerated memory deficit in diet-induced obese Alzheimer's disease mouse model. Nat Commun. 2023;14(1):1293.
70. Fischer F, Egg G. N-acetylneuraminic acid (sialic acid) as a tumor marker in head and neck cancers. HNO. 1990;38(10):361–3.
71. Firdous S, Abid R, Nawaz Z, Bukhari F, Anwer A, Cheng LL, Sadaf S. Dysregulated alanine as a potential predictive marker of glioma-an insight from untargeted HRMAS-NMR and machine learning data. Metabolites. 2021;11(8):507.
72. Chang S, Kim YH, Kim YJ, Kim YW, Moon S, Lee YY, Jung JS, Kim Y, Jung HE, Kim TJ, et al. Taurodeoxycholate increases the number of myeloid-derived suppressor cells that ameliorate sepsis in mice. Front Immunol. 2018;9:1984.
73. Režen T, Rozman D, Kovács T, Kovács P, Sipos A, Bai P, Mikó E. The role of bile acids in carcinogenesis. Cell Mol Life Sci. 2022;79(5):243.
74. Holeček M. Histidine in health and disease: metabolism, physiological importance, and use as a supplement. Nutrients. 2020;12(3):848.
75. Marcinkiewicz J, Kontny E. Taurine and inflammatory diseases. Amino Acids. 2014;46(1):7–20.
76. St Paul M, Saibil SD, Han S, Israni-Winger K, Lien SC, Laister RC, Sayad A, Penny S, Amaria RN, Haydu LE, et al. Coenzyme A fuels T cell anti-tumor immunity. Cell Metab. 2021;33(12):2415-2427.e2416.
77. Pham H, Vang K, Ziboh VA. Dietary gamma-linolenate attenuates tumor growth in a rodent model of prostatic adenocarcinoma via suppression of elevated generation of PGE(2) and 5S-HETE. Prostaglandins Leukot Essent Fatty Acids. 2006;74(4):271–82.
78. Nava Lauson CB, Tiberti S, Corsetto PA, Conte F, Tyagi P, Machwirth M, Ebert S, Loffreda A, Scheller L, Sheta D, et al. Linoleic acid potentiates CD8+ T cell metabolic fitness and antitumor immunity. Cell Metab. 2023;35(4):633-650.e639.
79. De Flora S, Izzotti A, D'Agostini F, Balansky RM. Mechanisms of N-acetylcysteine in the prevention of DNA damage and cancer, with special reference to smoking-related end-points. Carcinogenesis. 2001;22(7):999–1013.
80. Shi Z, Puyo CA. N-Acetylcysteine to combat COVID-19: an evidence review. Ther Clin Risk Manag. 2020;16:1047–55.
81. Williams NC, O'Neill LAJ. A role for the Krebs cycle intermediate citrate in metabolic reprogramming in innate immunity and inflammation. Front Immunol. 2018;9:141.
82. Ren JG, Seth P, Ye H, Guo K, Hanai JI, Husain Z, Sukhatme VP. Citrate suppresses tumor growth in multiple models through inhibition of glycolysis, the tricarboxylic acid cycle and the IGF-1R pathway. Sci Rep. 2017;7(1):4537.
83. Jong CJ, Sandal P, Schaffer SW. The role of taurine in mitochondria health: more than just an antioxidant. Molecules. 2021;26(16):4913.
84. Rao H, Liu C, Wang A, Ma C, Xu Y, Ye T, Su W, Zhou P, Gao W-Q, Li L, et al. SETD2 deficiency accelerates sphingomyelin accumulation and promotes the development of renal cancer. Nat Commun. 2023;14(1):7572.
85. Yuan L, Zhang F, Shen M, Jia S, Xie J. Phytosterols suppress phagocytosis and inhibit inflammatory mediators via ERK pathway on LPS-triggered inflammatory responses in RAW264.7 macrophages and the correlation with their structure. Foods. 2019;8(11):582.
86. Minamihata T, Takano K, Moriyama M, Nakamura Y. Lysophosphatidylinositol, an endogenous ligand for G protein-coupled receptor 55, has anti-inflammatory effects in cultured microglia. Inflammation. 2020;43(5):1971–87.
87. Loppi SH, Tavera-Garcia MA, Becktel DA, Maiyo BK, Johnson KE, Nguyen TV, Schnellmann RG, Doyle KP. Increased fatty acid metabolism and decreased glycolysis are hallmarks of metabolic reprogramming within microglia in degenerating white matter during recovery from experimental stroke. J Cereb Blood Flow Metab. 2023;43(7):1099–114.
88. Fromentin S, Forslund SK, Chechi K, Aron-Wisnewsky J, Chakaroun R, Nielsen T, Tremaroli V, Ji B, Prifti E, Myridakis A, et al. Microbiome and metabolome features of the cardiometabolic disease spectrum. Nat Med. 2022;28(2):303–14.
89. Stols-Gonçalves D, Mak AL, Madsen MS, van der Vossen EWJ, Bruinstroop E, Henneman P, Mol F, Scheithauer TPM, Smits L, Witjes J, et al. Faecal Microbiota transplantation affects liver DNA methylation in Non-alcoholic fatty liver disease: a multi-omics approach. Gut Microbes. 2023;15(1):2223330.
90. Kusy K, Matysiak J, Zarębska EA, Klupczyńska-Gabryszak A, Ciekot-Sołtysiak M, Plewa S, Kokot ZJ, Dereziński P, Zieliński J. Changes in plasma concentration of free proteinogenic and non-proteinogenic amino acids in high-performance sprinters over a 6-month training cycle. J Clin Med. 2024;13(17):5300.
91. Li X, Liu Y, Xu G, Xie Y, Wang X, Wu J, Chen H. Plasma metabolomic characterization of SARS-CoV-2 Omicron infection. Cell Death Dis. 2023;14(4):276.
92. Kaminski HJ, Andrade FH. Nitric oxide: biologic effects on muscle and role in muscle diseases. Neuromuscul Disord. 2001;11(6):517–24.
93. Tran GT, Hodgkinson SJ, Carter NM, Verma ND, Plain KM, Boyd R, Robinson CM, Nomura M, Killingsworth M, Hall BM. IL-5 promotes induction of antigen-specific CD4+CD25+ T regulatory cells that suppress autoimmunity. Blood. 2012;119(19):4441–50.
94. Tanaka T, Narazaki M, Kishimoto T. IL-6 in inflammation, immunity, and disease. Cold Spring Harb Perspect Biol. 2014;6(10):a016295.
95. Lee N, You S, Shin MS, Lee WW, Kang KS, Kim SH, Kim WU, Homer RJ, Kang MJ, Montgomery RR, et al. IL-6 receptor α defines effector

memory CD8+ T cells producing Th2 cytokines and expanding in asthma. Am J Respir Crit Care Med. 2014;190(12):1383–94.
96. Schumann J, Stanko K, Schliesser U, Appelt C, Sawitzki B. Differences in CD44 surface expression levels and function discriminates IL-17 and IFN-γ producing helper T cells. PLoS ONE. 2015;10(7):e0132479.
97. Alspach E, Lussier DM, Schreiber RD. Interferon γ and its important roles in promoting and inhibiting spontaneous and therapeutic cancer immunity. Cold Spring Harb Perspect Biol. 2019;11(3):a028480.
98. Huster KM, Busch V, Schiemann M, Linkemann K, Kerksiek KM, Wagner H, Busch DH. Selective expression of IL-7 receptor on memory T cells identifies early CD40L-dependent generation of distinct CD8+ memory T cell subsets. Proc Natl Acad Sci U S A. 2004;101(15):5610–5.
99. Hughes AM, Kuek V, Kotecha RS, Cheung LC. The bone marrow microenvironment in B-cell development and malignancy. Cancers (Basel). 2022;14(9):2089.
100. Liu Q, Sun Z, Chen L. Memory T cells: strategies for optimizing tumor immunotherapy. Protein Cell. 2020;11(8):549–64.
101. Farber DL, Yudanin NA, Restifo NP. Human memory T cells: generation, compartmentalization and homeostasis. Nat Rev Immunol. 2014;14(1):24–35.
102. Im S, Kim H, Jeong M, Yang H, Hong JY. Integrative understanding of immune-metabolic interaction. BMB Rep. 2022;55(6):259–66.
103. Thapa B, Lee K. Metabolic influence on macrophage polarization and pathogenesis. BMB Rep. 2019;52(6):360–72.
104. Bailey JD, Diotallevi M, Nicol T, McNeill E, Shaw A, Chuaiphichai S, Hale A, Starr A, Nandi M, Stylianou E, et al. Nitric oxide modulates metabolic remodeling in inflammatory macrophages through TCA cycle regulation and itaconate accumulation. Cell Rep. 2019;28(1):218-230.e217.
105. Puleston DJ, Buck MD, Klein Geltink RI, Kyle RL, Caputa G, O'Sullivan D, Cameron AM, Castoldi A, Musa Y, Kabat AM, et al. Polyamines and eIF5A hypusination modulate mitochondrial respiration and macrophage activation. Cell Metab. 2019;30(2):352-363.e358.
106. Yeh CL, Tanuseputero SA, Wu JM, Tseng YR, Yang PJ, Lee PC, Yeh SL, Lin MT. Intravenous arginine administration benefits CD4+ T-cell homeostasis and attenuates liver inflammation in mice with polymicrobial sepsis. Nutrients. 2020;12(4):1047.
107. Puleston DJ, Baixauli F, Sanin DE, Edwards-Hicks J, Villa M, Kabat AM, Kamiński MM, Stanckzak M, Weiss HJ, Grzes KM, et al. Polyamine metabolism is a central determinant of helper T cell lineage fidelity. Cell. 2021;184(16):4186-4202.e4120.
108. Chi H. Immunometabolism at the intersection of metabolic signaling, cell fate, and systems immunology. Cell Mol Immunol. 2022;19(3):299–302.
109. Hu T, Liu CH, Lei M, Zeng Q, Li L, Tang H, Zhang N. Metabolic regulation of the immune system in health and diseases: mechanisms and interventions. Signal Transduct Target Ther. 2024;9(1):268.
110. Luengo A, Gui DY, Vander Heiden MG. Targeting metabolism for cancer therapy. Cell Chem Biol. 2017;24(9):1161–80.

Publisher's Note